Available online at www.keaipublishing.com/en/journals/journal-of-magnesium-and-alloys/

ScienceDirect

Journal of Magnesium and Alloys 13 (2025) 5313–5344

www.elsevier.com/locate/jma

Review

Hydroxyapatite coatings for biodegradable magnesium alloys: Recent advances, strategies, challenges, and future prospects ☆

G. Suresh Kumar[a,*], K. Lalithambigai[b], Nguyen Van Minh[c,d,**], Mohd. Shkir[e,f], M.A. Sayed[e]

[a] *Department of Physics, PSG College of Arts & Science, Coimbatore, Tamil Nadu 641014, India*
[b] *Department of Physics, K.S.R. College of Engineering, Tiruchengode, Namakkal, Tamil Nadu 637215, India*
[c] *Institute of Research and Development, Duy Tan University, Da Nang, 550000, Vietnam*
[d] *School of Engineering & Technology, Duy Tan University, Da Nang, 550000, Vietnam*
[e] *Department of Physics, College of Science, King Khalid University, Post Box 960, Abha, 61421, AlQura'a, Saudi Arabia*
[f] *Smart Nano-Materials for Energy and Optoelectronic Devices Lab, Central Labs, King Khalid University, PO BOX 960, Abha, 61421, AlQura'a, Saudi Arabia*

Received 19 June 2025; received in revised form 18 September 2025; accepted 7 October 2025
Available online 14 November 2025

Abstract

Biodegradable magnesium (Mg) alloys have received increased attention as temporary medical implants due to their mechanical properties and density, similar to natural bone. However, the fast corrosion of Mg alloys in a physiological condition limits their wide applications. Hence, hydroxyapatite (HAp) coatings on Mg alloys have attracted much attention to address this corrosion issue and enhance the surface functionalities. In this paper, we present a review of HAp coating strategies on Mg alloys, including the sol-gel method, hydrothermal treatment, biomimetic coating, electrochemical deposition, electrophoretic deposition, and plasma electrolytic oxidation technique, and their recent progress to enhance the surface characteristics of Mg alloys. This review focused on aspects of coating morphology, hybrid formulations, and how they influence corrosion behavior as well as in vitro and in vivo performance. Moreover, we have discussed the future prospects of HAp-coating strategies, emphasizing on multifunctional, hybrid, and smart coatings for next-generation implant materials.

Keywords: Mg alloys; Hydroxyapatite; Coatings; Corrosion; Implants.

1. Introduction

Biodegradable magnesium (Mg) alloys have become promising materials for making temporary biomedical implants, especially in orthopedic and dental applications [1]. Mg-based alloys exhibits mechanical properties and density similar to natural bone. These features allow Mg alloys to provide adequate mechanical support without causing stress shielding [2,3]. Moreover, Mg is an essential element in the human body and plays a key role in metabolic and enzymatic functions. However, the fast corrosion rate of Mg alloys in physiological conditions remains a significant challenge [4–6]. This often leads to early loss of mechanical strength, localized hydrogen production, and unwanted biological reactions. Hence, addressing this problem is essential to maximizing the potential use of Mg-based biodegradable implants. One strategy developed to reduce corrosion and improve biological performance of Mg alloys making HAp coating on its surface [7,8]. As a bioactive ceramic with excellent properties for bone growth, HAp improves corrosion resistance and promotes bone bonding. Therefore, modifying the surface of Mg alloys with HAp has become a key area of research [7,8].

This review overviews recent advances in HAp coating methods for Mg alloys, such as sol-gel, hydrothermal treatment, biomimetic, electrochemical, electrophoretic deposition,

☆ Peer review under the responsibility of Chongqing University.

* Corresponding author at: Department of Physics, PSG College of Arts & Science, Coimbatore, Tamil Nadu 641014, India.
** Corresponding author at: Institute of Research and Development, Duy Tan University, Da Nang, 550000, Vietnam.
E-mail addresses: gsureshkumar1986@gmail.com (G.S. Kumar), nguyenvanminh15@duytan.edu.vn (N. Van Minh).

https://doi.org/10.1016/j.jma.2025.10.010

and plasma electrolytic oxidation. The focus is on coating structure, hybrid and composite formulations, and how this affects corrosion resistance and in vitro and in vivo performance. Finally, this review explores new possibilities, including multifunctional innovative coatings, bioactive interfaces for drug delivery, and additive manufacturing techniques like 3D-printed HAp-coated Mg scaffolds to enhance the potential applications of Mg alloys for orthopedic and dental bioresorbable implants.

2. Mg alloys in biomedicine

Metallic alloys are plays an important role in the biomedical implant industry. They have good mechanical strength, corrosion resistance, and biocompatibility, which are important for their applications [9]. Among these alloys, 316 L stainless steel is commonly used for load-bearing implants owing to its strong mechanical properties and low cost [10]. However, the main concern is the release of nickel and chromium ions [11]. Cobalt-chromium alloys are still preferred for load-bearing applications, like hip and knee replacements, because of their strong wear resistance and corrosion stability [12]. Titanium and titanium alloys, especially Ti-6Al-4V and Ti-6Al-7Nb, are used as a long-term orthopedic and dental implants owing to high biocompatibility, corrosion resistance, and good strength-to-weight ratio [13]. The excellent biocompatibility and corrosion resistance of zirconium-niobium (Zr-Nb) and tantalum (Ta) alloys make them potential candidates for next-generation implant materials [11,14]. Recently, magnesium-based alloys have attracted much attention as biodegradable implants that dissolve in the body while promoting new bone growth [1,15]. Improving metallic alloys through surface modification is crucial for boosting their biological performance and expanding their use in biomedical engineering.

As the lightest structural metal, Mg has drawn considerable attention for its potential in biomedical applications [16]. It is among the principal essential elements naturally participating in several physiological processes, such as cellular metabolism, enzymatic actions, protein synthesis, and neuromuscular function in the human body. This inherent biofunctionality highly corroborates Mg as a material for medical implants [17]. High natural abundance, low cost, and convenient mechanical properties make Mg as a promising alternative to traditional materials used in clinical applications [18,19]. In orthopedics and related medical fields, implant material is essential for the overall success of surgery and patient recovery. Materials such as traditional metallic implants made from titanium alloys, stainless steel, and cobalt-chromium alloys are the most commonly used choice for these implants because of their excellent mechanical strengths, corrosion resistance, and an established performance [20,21]. These implants are permanent and usually remain in the body long after the healing process. Unfortunately, removal of the implant is required in many cases, which needs another surgical procedure. Mg-based materials can effectively address this limitation [2,22].

One of the prominent characteristics of Mg alloys is their biodegradability in physiological conditions. Under the physiological environment, Mg slowly degrade to form magnesium hydroxide and hydrogen gas. The body then absorbs or excretes these products. These unique self-degrading characteristics permit Mg-based implants to gradually dissolve as the regenerated surrounding tissue replaces the implant, thus eliminating the need for surgical removal and reducing the overall burden on healthcare systems [22–24]. Fig. 1 depicts an essential correlation between the degradation rate of Mg implants and their mechanical strength with bone healing. Initially, Mg implants provide sufficient mechanical support to stabilize fractured bone. As healing progresses, the implant is loose while the bone gains strength. This provides support only through healing without unnecessary retention of foreign materials in the body [4].

Mg alloys are biodegradable and also show good biocompatibility. This property is essential for materials used in medical applications [22,23]. Many in vitro and in vivo studies have shown that the body tolerates Mg and its degradation products, resulting in little inflammatory response and favorable interaction with surrounding tissues [2,22,25,26]. Mg ions play an essential role in bone remodeling and regeneration, thus making them very suitable for Mg-based implants in orthopedic and dental applications [2,3]. Fig. 2 shows a diagram of how Mg alloys help bone healing by changing immune responses, improving blood vessel formation, supporting bone growth, and controlling osteoclast activity when used as bone implants. The elastic modulus for Mg is very similar to that of human bone [3,27]. Table 1 compares Mg-based alloys, pointing out the differences in mechanical properties based on their composition [4]. These differences highlight how alloy composition is crucial for developing Mg-based materials in biomedical implant applications [4]. These differences emphasize the importance of alloy composition in optimizing Mg-based materials for biomedical implant applications. Thus, by more closely simulating the mechanical behavior of bone, Mg alloys would help in the natural load distribution and rehabilitation of bone [3,27]. A long-term clinical study conducted by Lee et al. demonstrated the effectiveness of biodegradable Mg-5wt%Ca-1wt%Zn alloy implants in orthopedic applications [28]. This matrix initiates early bone healing and enables complete replacement of the Mg alloy with natural bone within 1 year. This study, involving 53 successful clinical cases, highlights the potential of Mg-based alloys as next-generation bioresorbable implants for skeletal repair [28].

The biomedical use of Mg alloys includes orthopedics for temporary fixation devices, cardiovascular systems as biodegradable stents, and new areas like tissue engineering scaffolds and localized drug delivery [2,25,29]. However, controlling corrosion is still the most significant challenge [1,30]. In an aqueous solution, Mg experiences electrochemical corrosion as follows.

$$Mg \rightarrow Mg^{2+} + 2e^{-}$$

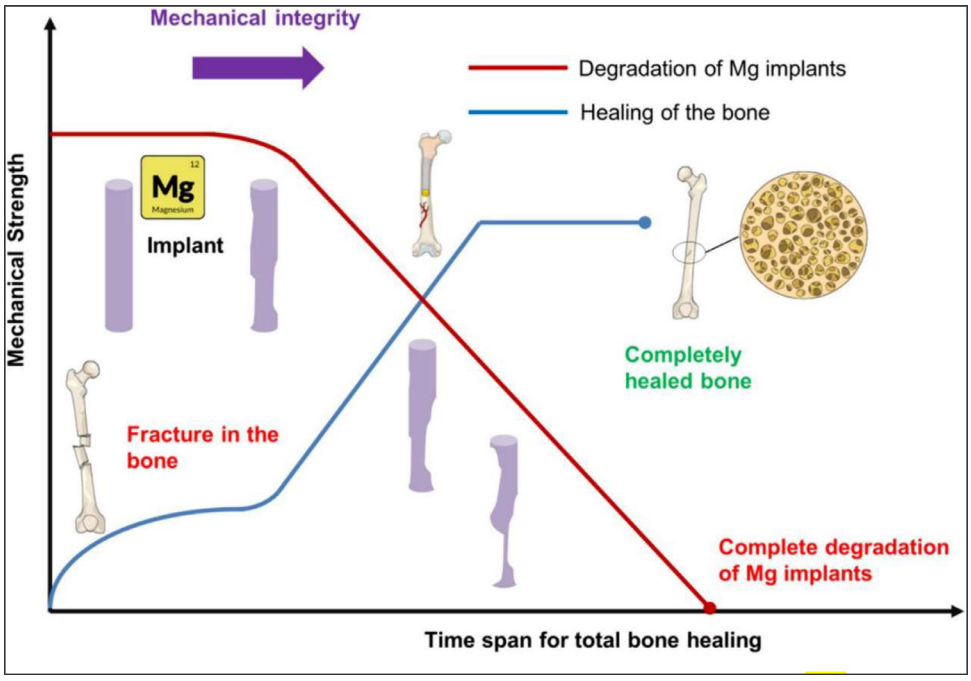

Fig. 1. Relationship between the mechanical strength, degradation of Mg implants, and bone healing time (Reproduced with permission from Ref. [4]. License no: 6050031331795).

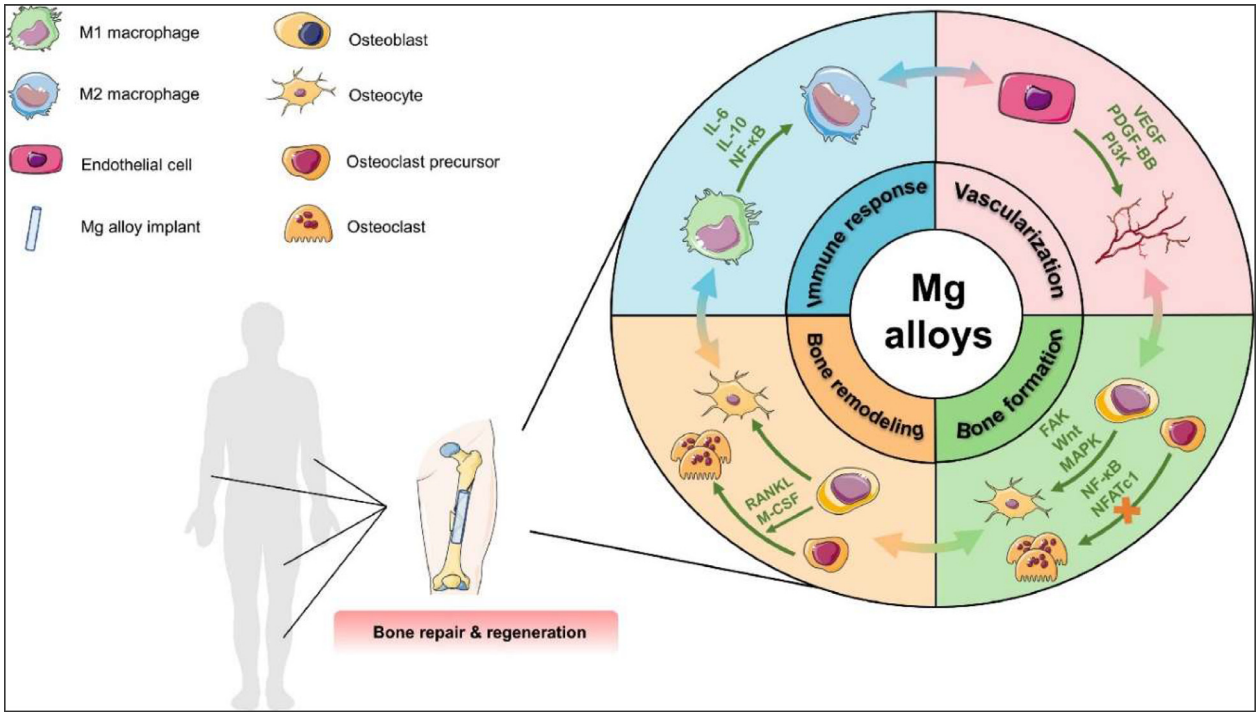

Fig. 2. Schematic illustration of Mg alloys on participating immune response, angiogenesis, osteogenesis, and regulation of osteoclast function as bone implants to drive bone healing. Reproduced under Creative Commons license from Ref. [25].

$$2H_2O + 2e^- \rightarrow H_2\uparrow + 2OH^-$$

$$Mg^{2+} + 2OH^- \rightarrow Mg(OH)_2\downarrow$$

$$Mg(OH)_2 + 2Cl^- \rightarrow MgCl_2 + 2OH^-$$

This process may lead to fast corrosion, which creates Mg^{2+} ions and hydrogen gas at the implanted sites. Fig. 3 shows the different corrosions products formed under physiological conditions and the related chemical reactions [29]. Although Mg's biodegradability eliminates the need for secondary implant surgeries. However, its degradation rate needs

Table 1
Mechanical properties of pure Mg and Mg-based alloys compared with bone [1,4].

Materials	Yield strength (MPa)	Tensile strength (MPa)	Elongation to break (%)
Bone	104–121	110–130	0.7–3
Pure Mg	65–100	90–190	2–10
AZ31	185	263	15–23
AZ91	160	150	2.5–11
WE43	170	220	2–17
Mg-Ca	110	220	15
Mg-Zn	95	200	10
M-Sr	80	180	12
Mg-Y	115	230	8
Mg-Zn-Ca	105	210	9
Mg-Zn-Mn	90	195	13
Mg-Zn-Sr	100	205	7
Mg-Ca-Zn	108	220	6
Mg-Zn-Sc-Sr	103	210	9

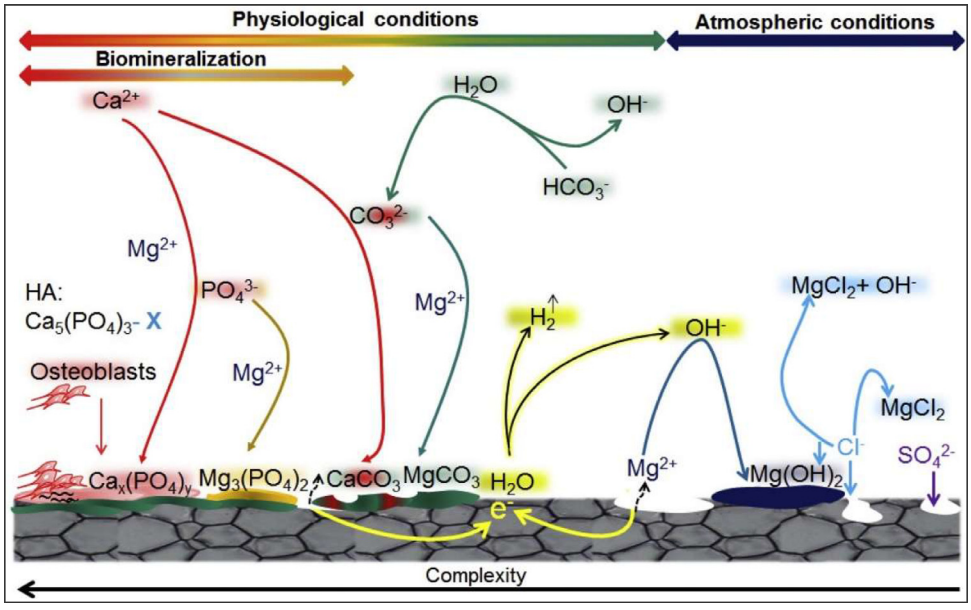

Fig. 3. Degradation products formed under physiological conditions and the corresponding chemical reactions. Reproduced under Creative Commons license from Ref. [31].

careful control. Too rapid corrosion might cause the implant to lose its mechanical integrity before the surrounding tissue has sufficiently healed. This early failure could cause total mechanical collapse, implant loosening, or incomplete bone regeneration in load-bearing applications. Another significant concern is the rapid release of hydrogen gas during corrosion. Small amounts of hydrogen gas can be either dissolved into the bloodstream or absorbed into nearby tissues [30,31]. On fast degradation, however, the accumulation of large amount of hydrogen can create gas cavities around the implant site. These gas cavities might hinder osseointegration, interfere with tissue healing, cause soft tissue separation, or localized pressure effects.

Several researchers have investigated the different approaches to address corrosion challenges by creating new Mg alloys, surface modification, and protective coatings [32,33]. Combining magnesium with calcium, zinc, manganese, and rare earth elements can improves corrosion resistance and mechanical strength with biocompatibility. Micro-arc oxidation, plasma electrolytic oxidation, and bioceramic coatings have also shown promising results in controlling the degradation rate and improving cell adhesion and tissue integration [3,34]. One of the widely explored methods is surface protective coating using bioactive ceramics. Among these, the application of HAp coatings has received significant attention. HAp is a naturally occurring mineral form of calcium apatite, chemically similar to the inorganic component of bone, and exhibits excellent biocompatibility and osteoconductivity [35]. We can create a barrier by coating Mg implants with HAp that can reduce the corrosion rate while enhancing bone cell attachment and growth [7].

3. Overview of HAp: structure, properties, and biological significance

Calcium phosphates are bioceramics of different types whose properties mainly depend on their calcium/phosphorus (Ca/P) molar ratios that affect solubility, stability, and bioac-

Table 2
Stoichiometric compositions and Ca/P molar ratios of various calcium phosphate compounds [36–38].

Compound name	Chemical formula	Ca/P ratio	Solubility	Characteristics & applications
MCPM	$Ca(H_2PO_4)_2{\cdot}H_2O$	0.50	High	Dental cements, fertilizer, food additives
DCPD	$CaHPO_4{\cdot}2H_2O$	1.00	Moderate	Bone repair, resorbable cements, drug delivery
DCPA	$CaHPO_4$	1.00	Low	Toothpaste additive, dental cements, food additive
OCP	$Ca_8H_2(PO_4)_6{\cdot}5H_2O$	1.33	Moderate	Bone graft substitute, precursor to HAp in biomineralization
ACP	$Ca_9(PO_4)_6{\cdot}nH_2O$	~1.50	Variable	Tooth remineralization, coatings, and controlled drug release
β-TCP	β-$Ca_3(PO_4)_2$	1.50	Moderate	Bone grafting, bioresorbable scaffolds, and dental cements
α-TCP	α-$Ca_3(PO_4)_2$	1.50	High	Self-setting bone cements, precursor to HAp
HAP	$Ca_{10}(PO_4)_6(OH)_2$	1.67	Very low	Orthopedic implants, dental implants, bone fillers, coatings
TTCP	$Ca_4(PO_4)_2O$	2.00	Moderate	Dental restorative materials, self-setting cements

tivity. Table 2 presents a comparative overview of the chemical compositions and corresponding Ca/P ratios of different calcium phosphate compounds [36,37]. These compounds are commonly used in different biomedical applications due to their relevance to biological mineralization and bone-like materials. Inorganic salts of lesser Ca/P ratios like monocalcium phosphate monohydrate (MCPM), dicalcium phosphate dihydrate (DCPD), and dicalcium phosphate anhydrous (DCPA) are soluble and therefore serve well in resorbable types of applications. Octacalcium phosphate (OCP) and amorphous calcium phosphate (ACP) represent metastable phases in early-stage bone mineralization. Tricalcium phosphate (TCP) has intermediate solubility and finds use in bone grafts. HAp is the most stable and bioactive phase, thus preferred in long-term implantations. Tetracalcium phosphate (TTCP) is more reactive makes it suitable for use in bone cements. The knowledge of variations in Ca/P ratio thus becomes key factor to designing materials for specific biomedical applications [36,37].

Among different calcium phosphate phases, HAp is the most stable and biologically relevant calcium phosphate phase since it is main mineral constituents of human bone and teeth [37,39,40]. Due to its biocompatibility, osteoconduction, and solubility under physiological conditions, HAp finds wide applications in orthopedics and dentistry as a bone substitute, implant coating, and scaffold in tissue engineering. Human mineralized tissues (enamel, dentin, and bone) differ significantly in composition to fulfill their physiological functions. Enamel is the outer layer of the teeth and is highly mineralized (~95–97% inorganic), with a negligible amount of organic matrix and water. Hence, enamel is the hardest tissue in the body. On the other hand, dentin and bone are relatively poorly mineralized, with approximately 70% and 60–70% mineral content, respectively, and contain large amounts of type I collagen and water [41–43]. Table 3 provides a comparative summary of the major elemental constituents found in three mineralized tissues of the human body [38,44]. All three tissues primarily comprise carbonated HAp, with Ca/P molar ratio close to 1.67 [42,45]. Moreover, mineralized tissues contains several trace elements, such as fluoride, magnesium, sodium, strontium, zinc, and carbonate. These trace elements influence the minerals' crystallinity, solubility, and mechanical properties. Fluoride enhances enamel's resistance to acids, while Mg and strontium are essential stimulators of

Table 3
Typical elemental composition of human enamel, dentin, and bone tissues [38,44].

Component	Enamel	Dentine	Bone
Calcium (Ca)	37.60	40.30	36.60
Phosphorus (P)	18.30	18.60	17.10
Carbon dioxide (CO_2)	3.00	4.80	4.80
Sodium (Na)	0.70	0.10	1.00
Potassium (K)	0.05	0.07	0.07
Magnesium (Mg)	0.20	1.10	0.60
Strontium (Sr)	0.03	0.04	0.05
Chlorine (Cl)	0.40	0.27	0.10
Fluorine (F)	0.01	0.07	0.10
Ca/P molar ratio	1.59	1.67	1.65

in vivo bone formation and regeneration. The unique compositional features of each tissue highlight the importance of tailoring biomimetic materials for dental and orthopedic applications [42,46].

Bone is indeed a hierarchical and intricate biological material with structural organization occurring in several different length scales from macro to nano. The schematic illustration of bone structure is shown in Fig. 4 [42,47]. At the macroscopic level, bone is classified as cortical or cancellous based on its density and porosity. The basic structural units of cortical bone are osteons (100–200 μm in diameter). Osteons is formed by lamellae, with diameters in the 3–7 μm range surrounding a central Haversian canal that supports nutrient exchange. The lamellae are made of collagen fiber bundles approximately 500 nm in diameter on a nanoscale. Nano-sized HAp crystals, roughly 50 nm in length, located within and between the collagen fibers, impart stiffness and compressive strength to the bone [42,48]. These highly oriented HAp crystals are tightly associated with tropocollagen molecules–triple-helical protein strands of about 1.5 nm in diameter that self-assemble into fibrils and function as a matrix template for mineral deposition. Collagen is rigid and elastic, whereas HAp crystals are hard and brittle. Together, they produce a great composite that is both strong and resilient [47,48]. This delicate multi-scale architecture allows bone to carry diverse mechanical loads while performing its physiologic functions of support, protection, and mineral storage. The structural and chemical similarity between synthetic HAp and biological apatite leads to its extensive application in hard tissue engineering, dental restoration, and orthopedic implants.

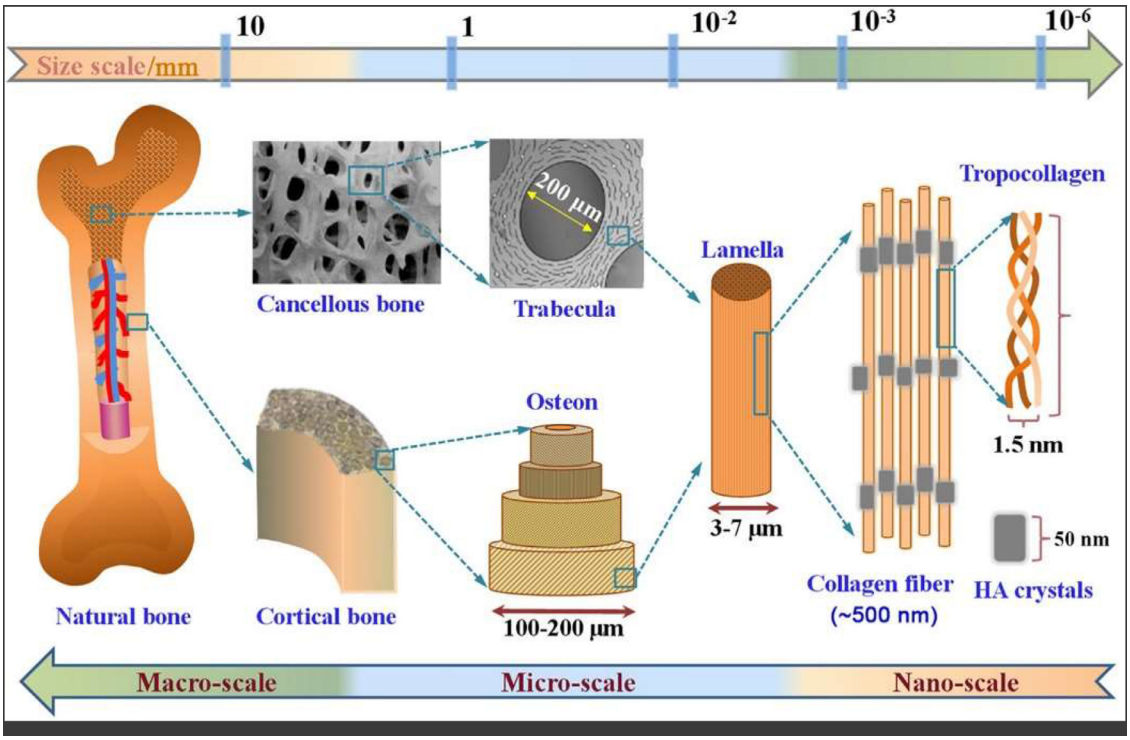

Fig. 4. The hierarchical structure of bone from macroscale to nanoscale. Reproduced under Creative Commons license from Ref. [47].

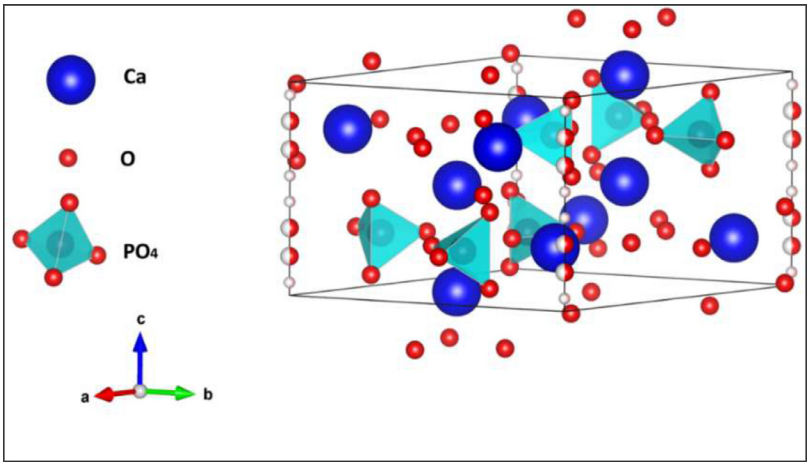

Fig. 5. Hexagonal crystal structure of HAp, illustrating the arrangement of calcium (Ca^{2+}), phosphate (PO_4^{3-}), and hydroxyl (OH^-) ions within the unit cell (obtained by software VESTA [52]).

The crystal structure of HAp is shown in Fig. 5. It has a hexagonal structure with space group $P6_3/m$ and unit cell parameters $a = b \approx 9.42$ Å and $c \approx 6.88$ Å [44,49–51]. It consists of calcium ions (Ca^{2+}), phosphate groups (PO_4^{3-}), oxygen atoms (O), and hydroxyl ions (OH^-). The calcium ions occupy two different types of sites (Ca(I) and Ca(II)). The Ca(I) site is coordinated by nine oxygen atoms emanating from phosphate groups, whereas the Ca(II) site is coordinated by six oxygen and one hydroxyl ion to form a seven-fold coordination. The phosphate tetrahedra are evenly distributed throughout the structure, interacting with calcium ions to stabilize the lattice. The hydroxyl ions tend to be ordered in channels parallel to the c-axis [44,50,51]. This stable structure allows substituting trace elements naturally present in biological apatite, including carbonate, fluoride, sodium, magnesium, and strontium [42]. The ionic substitutions in HAp can improve the mineral's biological nature by modifying the solubility, crystallinity, and interaction with biological fluids. Ca/P ratio of 1.67 is important in maintaining the stoichiometry of HAp and hence its biofunctionality [37]. A ratio other than these might result in a calcium-deficient apatite or the presence of other calcium phosphate phases like TCP, influencing its resorption behavior and cellular responses [36,40].

Table 4
HAp synthesis methods, resulting morphologies, and their biomedical significance.

Synthesis method	Resulting morphology	Key parameters (e.g., temp, pH)	Ker characteristics	Biomedical applications
Wet chemical Precipitation	Rod-like, needle-like	pH ∼10, temp ∼37–90 °C	High surface area, good biocompatibility	Bone scaffolds, coatings on implants
Sol-gel method	Nanoparticles, spherical	pH ∼above 9, calcination at ∼600 °C	High purity, uniform size, bioactivity	Drug delivery, dental fillers
Hydrothermal synthesis	Nanorods, nanowires	Temp ∼120–200 °C, pressure >1 atm	High crystallinity, anisotropic growth	Load-bearing bone tissue engineering
Microwave-assisted synthesis	Nanoplates, nanospheres	Short time, pH ∼above 9, temp ∼150 °C	Rapid crystallization, uniform morphology	Fast bone regeneration, injectable bone pastes
Ultrasound-assisted synthesis	Flower-like, porous structures	Frequency ∼20–40 kHz, temp ∼25–60 °C	High porosity, improved drug loading	Local drug delivery, anti-cancer delivery platforms
Spray drying	Spherical microparticles	Atomization, temp ∼100–150 °C	Controlled size, good dispersibility	Powdered formulations, bioresorbable carriers
Micro-emulsion technique	Porous spheres	Oil-water ratio, surfactants	High surface area, controlled pore structure	Controlled drug release, scaffold materials
Template-assisted synthesis	Hollow spheres, tubes	Use of soft/hard templates	Tailored pore structure, drug encapsulation	Targeted drug delivery, regenerative scaffolds
Electrochemical deposition	Oriented nanorods/nanoplatelets	Voltage, electrolyte concentration	Strong adhesion, directional growth	Coatings on orthopedic and dental implants
Biomimetic synthesis	Plate-like, hierarchical	SBF, temp ∼37 °C	Close to natural bone composition	Bone graft substitutes, osteoinductive materials

HAp's physicochemical properties make it one of the prime material for biomedical applications [53,54]. Being highly biocompatible, HAp, when implanted in vivo, does not produce an immune or toxic response. This biocompatibility is due to its compositional similarity to the bone mineral, allowing it to integrate with host tissue [39,46]. The term "bioactivity" refers to the ability of HAp to form a direct bond with bone tissue [55,56]. This direct bonding happens when HAp surfaces stimulate a biological apatite layer upon implantation, facilitating cell adhesion. This bioactivity also allows osteoconduction to occur along the HAp material's surface, which bonds itself to the surrounding skeletal structure. Osteoconduction implies that HAp can provide a framework for osteoblast proliferation that form new bone tissue [57,58]. Further, HAp could be osteoinductive in particular forms or compositions, especially if combined with growth factors or employed in a nanoscale morphology [53,54]. When designing structural implants for load-bearing applications, it's essential to consider the mechanical properties of HAp. In non-load-bearing cases, HAp usually offers enough support [56]. HAp is brittle and possesses low fracture toughness and tensile strength [42,53]. Hence, HAp is combined with polymers, metals, and ceramics to overcome the above drawbacks and achieve better mechanical properties while maintaining its biological properties [58,59].

HAp surface offers binding sites for protein and growth factor, providing a bioactive interface for adhesion of cells and their differentiation into osteoblasts [42,60,61]. Besides enhancing cell adhesion, certain ionic releases from HAp, especially calcium and phosphate ions, mediate signalling pathways regulating bone metabolism [60–62]. From the perspective of regenerative medicine, combining HAp with biological agents presents an excellent promise for tissue regeneration. HAp also acts as a carrier for delivering antibiotics, anti-inflammatory drugs, and osteoinductive proteins [63–65]. Its porous nature and biocompatibility offer localization and sustained release of therapeutics, which decreases systemic side effects and facilitates local tissue repair. Furthermore, when used as a scaffold, they may provide both the structural matrix and biological signals for efficient bone regeneration in large or complex defects [53,54].

HAp morphology significantly influences its performance in biomedical applications. Using different synthesis methods such as wet chemical precipitation, sol-gel, hydrothermal, microwave-assisted, and biomimetic approaches, we can tailor HAp into various structures like rods, spheres, plates, or porous structures. These morphologies can affect key properties such as surface area, crystallinity, porosity, and mechanical strength. Hence, we can develop HAp for specific applications through morphology tuning. Table 4 illustrates the different methods for synthesizing HAp nanostructures with different morphological characteristics. Fig. 6 illustrates diverse HAp nanostructures synthesized via various methods, including nanoneedles [66], nanowires [66,67], whiskers [68], nanorods [68], ultralong nanofibers [69], nanotube [70], nanosheets [71], nanobelts [72], brush-like structures [73], agglomerated microspheres [69], flower-like spheres [74], hierarchical nanosheet microspheres [75], hollow nanorod microspheres [75], bowknot-like nanosheets [76], and sea-cucumber-like structures [77]. Each morphology offers unique properties such as high surface area, porosity, and mechanical strength, making them suitable for specific biomedical applications like bone regeneration, drug delivery, and implant coatings [7,57,63,78]. Thus, morphology-controlled synthesis of HAp is essential for optimizing its functionality in applications such as bone grafts, implant coatings, tissue scaffolds,

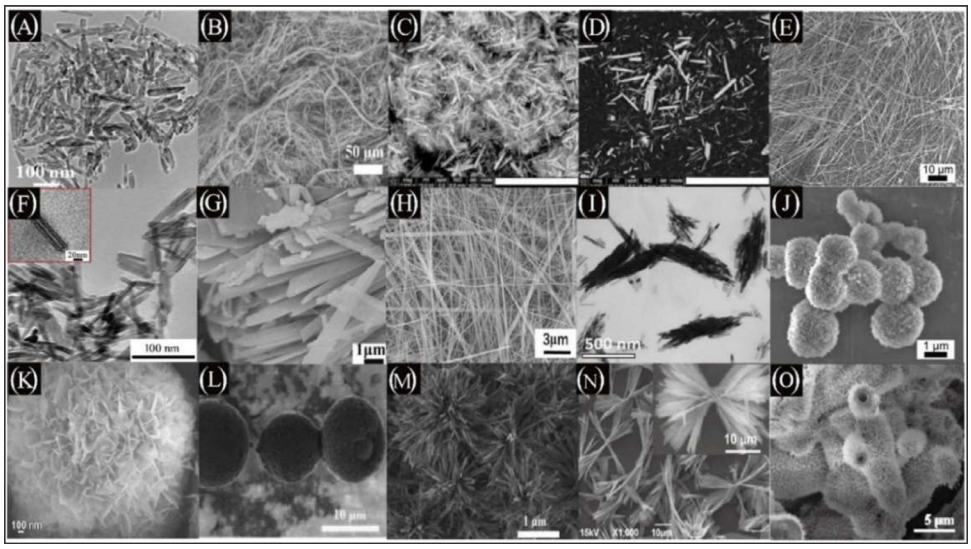

Fig. 6. HAp nanostructures with various morphologies: (A) nanoneedles, (B) nanowires, (C) whiskers, (D) nanorods, (E) ultralong nanofibers, (F) nanotubes, (G) nanosheets, (H) nanobelts, (I) brush-like structures, (J) agglomerated microspheres, (K) flower-like spheres, (L) hierarchical nanosheet microspheres, (M) hollow nanorod microspheres, (N) bowknot-like nanosheets, (O) sea-cucumber-like structures (Reproduced with permission from [61]. License no: 6050040137930).

and drug delivery systems. Moreover, HAp is combined with biodegradable polymers such as polylactic acid, polyglycolic acid, and polycaprolactone in scaffold composites to provide mechanical flexibility and competent bioactivity [79,80]. HAp acts as a reinforcing phase in polymer matrices, enhancing mechanical properties and supporting bone cell interaction. Also, there is much interest in nanostructured HAp owing to its greater closeness to the nanoscale mineral platelets of natural bone. Nano-HAp, with its higher surface area, also exhibits enhanced protein adsorption and subsequently promotes cellular interactions compared to its microcrystalline counterpart [48]. Moreover, HAp substituted with rare earth ions can find applications in biomedical imaging such as CT, MRI, and fluorescence imaging [51,81]. These different applications show how HAp is flexible in addressing problems in orthopedics, dentistry, tissue engineering, drug delivery, and cancer diagnosis.

4. Coating techniques for HAp on Mg alloys

Mg alloys have received much attention amongst biomedical implants due to their excellent biodegradability and good mechanical properties. However, they are limited in use due to their rapid corrosion in physiological environments [82,83]. The best strategy proposed for protecting Mg-based materials from corrosion is the surface coating of HAp. Over the years, various coating methods have been developed for depositing HAp on Mg and Mg alloys. Different methodologies are vastly varied in complexity and cost, processing conditions, and also differ in the parameters of corrosion resistance, mechanical properties, adhesion strength, and biological activity of the Mg alloys. Most used coating techniques are sol-gel coating, biomimetic process, hydrothermal process, electrochemical deposition, electrophoretic deposition, plasma electrolytic oxidation (PEO), and RF magnetron sputtering [84,85].

4.1. Sol-gel technique

The sol-gel method has become one of the facile techniques to produce HAp coatings on metal alloy substrates because of its simplicity, cost-effectiveness, and nanostructure production [86–88]. In this method, calcium and phosphate precursors were dissolved in a suitable solvent with the addition of a complexing or pH-controlling agent to form a stable sol by controlled hydrolysis and polycondensation reactions. The resulted sol containing dispersed HAp precursors could be deposited on the Mg alloy surface by different methods such as dip coating, spin coating, and spray coating. Dip coating immerses the substrate in the sol and then slowly withdraws it, while spin coating spins the substrate at high speeds to spread the sol evenly on its surface. Spray coating covers large or uneven surfaces quite well. The deposited coating is then heat treated to remove residual organics and stimulate crystallization for better adhesion. The sol-gel coating of HAp on Mg alloy mostly uses calcium nitrate and triethyl phosphate as precursors, which form a gel that is applied and heat-treated to create a uniform HAp layer [87]. Fig. 7(a) shows a typical schematic illustration of the sol-gel process used to fabricate HAp coatings on a Mg alloy substrate. Cross-sectional view of HAp coating fabricated through sol-gel method on AZ91 magnesium alloy by Rojaee et al. is shown in Fig. 7(b) [89], revealed thin, dense, and homogeneous coating.

Sol-gel processing is popular for applying HAp coatings on Mg alloys because it can alter chemical compositions and microstructures, provide selective coatings to complex shapes, operate at lower temperatures, and protect substrates from structural alterations [86,88]. This process results in thin,

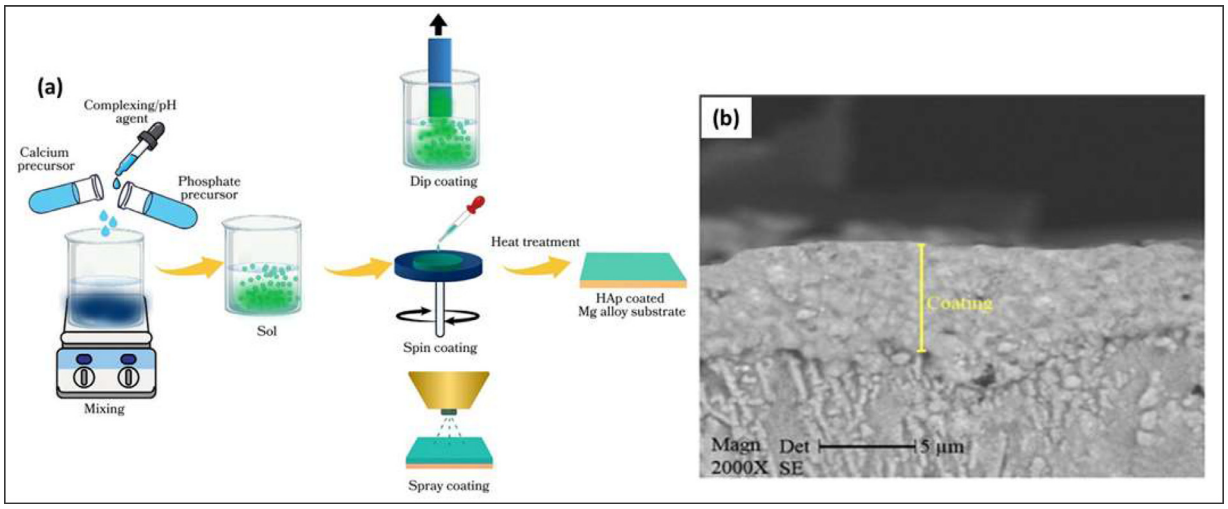

Fig. 7. (a) Schematic illustration of a typical sol-gel process for fabricating HAp coatings on Mg alloy substrate. (b) Cross-sectional view of HAp coating fabricated by the sol-gel method on AZ91 magnesium alloy, as reported by Rojaee et al. (Reproduced with permission from Ref. [89], License no: 6104150168439).

dense, and homogeneous coatings with a porous texture and surface area adjustable to orthopedic implants requiring surface bioactivity and controlled degradation. However, maintaining the viscosity of the sol, drying rate, and thermal treatment is necessary to prevent the formation of cracks, ensure homogeneity, and maintain thickness. Surface pretreatments such as acid etching and micro-arc oxidation can further enhance adhesion by increasing the roughness of the substrate [86–88,90].

Several studies have explored applying sol-gel derived HAp coatings on Mg alloys with promising results. Rojaee et al. effectively developed an n-HAp coating using the sol-gel method on the AZ91 Mg alloy [89]. The n-HAp layer formed through careful dip-coating and calcination at 400 °C was uniform. This coating provided good corrosion resistance, controlled Mg^{2+} ion release, and stabilized local pH levels. Thus, the coating enhanced osteoblast activity and bone regeneration. Singh et al. coated Mg-3Zn alloys with HAp, considering the surface roughness of 15–20 nm to enhance coating adhesion [91]. They obtained sintered HAp coatings with dense, and strong interfacial bonding. They reported a highly increased resistance to corrosion by 40 times compared to the bare Mg alloy with higher osteoblast proliferation and adhesion. Further, Ye et al. explores the effect of mesoporous HAp coatings in enhancing corrosion resistance of AZ31 Mg alloy to obtain a potential material for biodegradable implants [92]. Using the sol-gel dip-coating technique, mesoporous HAp coatings were applied and compared with uncoated samples and samples coated with non-mesoporous HAp. This study points out that with mesoporous HAp coatings, corrosiveness and bioactivity can be balanced efficiently, thereby proposing an interesting approach to prolong the working life and biocompatibility of Mg-based orthopedic devices. Larimi et al. coated Mg-Zn-Ca alloys with composite HAp-bone powder coatings to promote further developments in sol-gel coatings [93]. Anodization in NaOH and Na_2SiO_3 was employed to form a porous MgO interlayer to enhance coating adhesion. The HAp and bone powder provided a twofold barrier against corrosion and bioactivity, highlighting the synergistic effect of composite layers for orthopedic applications. Roy et al. further contributed to this field by laying porous calcium phosphate coatings on Mg4Y alloys [94]. The most innovative work by Singh et al. where they produced a double-layer superhydrophobic coating with self-healing property over Mg-Ag-Zn-Ca alloys [95]. The coating combining HAp, polycaprolactone (PCL), phytic acid (PA), and stearic acid showed excellent superhydrophobicity. The developed coating has good cytocompatibility and antibacterial efficacy for a multifunctional application against corrosion, mechanical wear, and bio-integration. It is clear from the series of above studies that HAp-based coatings from both pure and composite materials from sol-gel methods have consistently improved Mg alloys' corrosion resistance, bioactivity, and cytocompatibility for orthopedic applications. Such coatings act as a barrier to control diffusion and modulation of ion release, support osteoblast adhesion, and, to some extent, are antibacterial and self-healing. Moreover, surface pretreatments, hybrid coatings, and incorporating biopolymers or nanoparticles might be promising key factors to develop efficient HAp coating by the sol-gel process [87,88,90].

4.2. Hydrothermal method

The hydrothermal method involves crystallizing various materials from their aqueous solutions at high temperature and pressure in a sealed autoclave vessel [97–99]. It usually works at temperatures in the range of 100–300 °C. The hydrothermal method is one of the interesting approaches to deposit HAp coatings on Mg alloys to increase corrosion resistance and biocompatibility of implants for specific biomedical applications [100]. The main concept of this technique is to

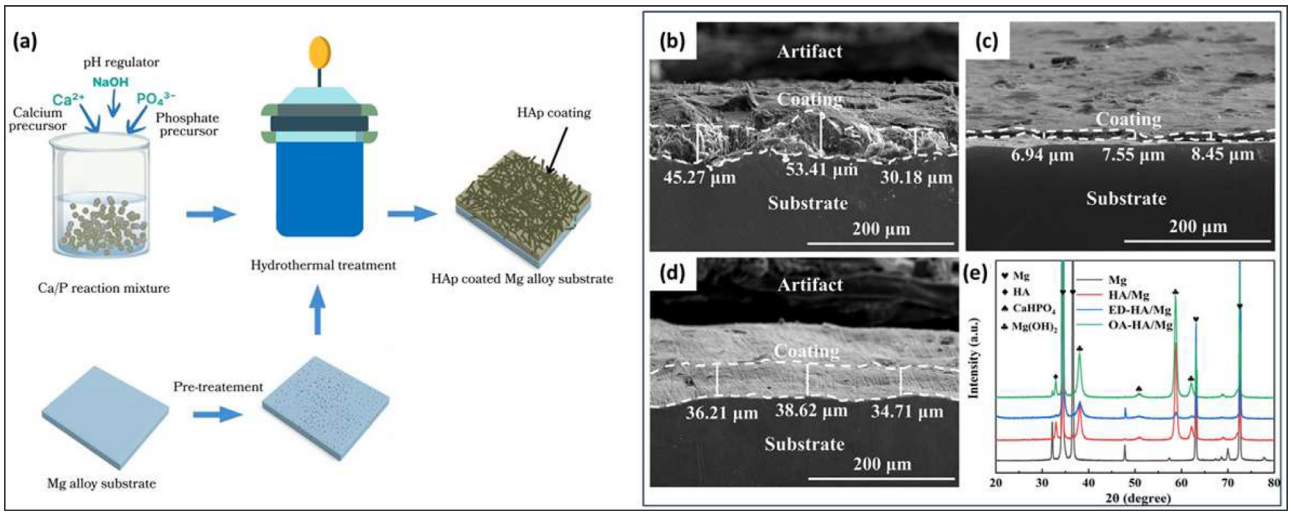

Fig. 8. (a) Schematic of a typical hydrothermal process for fabricating HAp coatings on Mg alloy substrate. Cross-sectional SEM images of (b) HAp, (c) ED templated HAp, (d) OA templated HAp coating on Mg alloy fabricated by hydrothermal process, and (e) their corresponding XRD patterns (Reproduced with permission from Ref. [96], License no:6143540487116).

immerse the Mg alloy substrate in an aqueous solution containing calcium and phosphate precursors, keeping it under elevated temperature and pressure within a sealed chamber. The hydrothermal conditions promote nucleation and growth of crystalline HAp on the Mg surface to form a uniform and adherent coating. It is possible to manipulate the crystallinity, morphology, and thickness of the HAp layer to tailor surface properties for enhanced in vivo performance of Mg-based implants. Solution parameters such as pH, temperature, reaction time, and precursor concentration are under exact regulations to control the microstructure and biofunctionality of the coating. Hydrothermal treatments offer coatings that are quite uniform and good crystallinity [78,100,101]. The hydrothermal method promotes the formation of well-crystallized HAp of controlled morphology that typically occurs in needle-like or plate-like forms, thus imparting surface roughness and biological activity [100,101]. The schematic illustration of the hydrothermal process for fabricating HAp coatings on Mg alloy substrate is shown in Fig. 8(a). Wen et al. systematically investigated the effect of precursor concentration, Ca/P ratio, reaction temperature, and time on microstructure and corrosion resistance of HAp coatings prepared on AZ31B Mg alloys. They observed distinctive flake-like morphologies that significantly enhance corrosion resistance [100]. The chemical modification of surfaces before the hydrothermal process brings an important key factor in hydrothermal coating. Gao et al. compared ethylenediamine (ED) and octanoic acid (OA) to examine the impact of organic templating agents on HAp coating. Fig. 8(b) revealed the microstructure and crystalline characteristics of HAp coating, revealing the role of carboxylic acid treatment in producing denser and more compact coating [96]. Jiang et al. also investigated additional functionality by adding polyelectrolytes during the hydrothermal synthesis of HAp coatings to form interpenetrating polymer–inorganic networks simultaneously. These networks offer compactness and mechanical integrity to the coatings. This study provided a potential method for addressing corrosion resistance and mechanical strength related to biodegradable Mg implants [102]. Peng et al. have used silane coupling agents of various functional groups (-NH_2, epoxy, vinyl) to modify the Mg substrate-based surface to fine-tune the binding ability toward Ca^{2+} and the nucleation behavior accordingly [103]. Fig. 9 shows the morphological feature and chemical composition of the silane-treated AZ31 Mg alloys coated with the HAp/$Mg(OH)_2$ coating via hydrothermal synthesis. The silane surface's top views (a_1–c_1) show a smooth surface, (a_2–c_2) show the sea urchin-like HAp structures. The cross sections (a_3–c_3) show the bilayer HAp/$Mg(OH)_2$ coating consisting of two elemental layers in which the silane type would influence the coating thickness, structure, and corrosion resistance. APTES-treated surfaces provide a moderate binding of Ca^{2+} that favored thicker bilayered coatings with an inner $Mg(OH)_2$ layer and an outer sea urchin-like HAp nanostructure. This structure improved corrosion resistance and bioactivity, through hierarchical architecture and compositional gradients [103]. Addressing biological issues, hybrid coatings combined HAp and antibacterial agents and bioactive molecules to fight implant infections while fostering osteogenesis. Zheng et al. produced layered double hydroxide/HAp composite coatings loaded with ciprofloxacin via hydrothermal routes. This coating successfully killing bacteria, biocompatible to osteoblasts, and promoting the expression of osteogenic markers, thus emphasizing a dual function for infection control and bone regeneration [104]. Likewise, Liao et al. developed HAp/tea polyphenol composite coatings that have HAp bioactivity with the antibacterial properties of tea polyphenol. This coating offer good corrosion resistance and promote osteoblast proliferation and biomimetic mineralization [105]. Moreover, Zhang et al. investigated HAp/palmitic acid composite coatings which exhibited good corrosion resistance in simulated body fluids and >98% antibacterial efficiency against common pathogens [106].

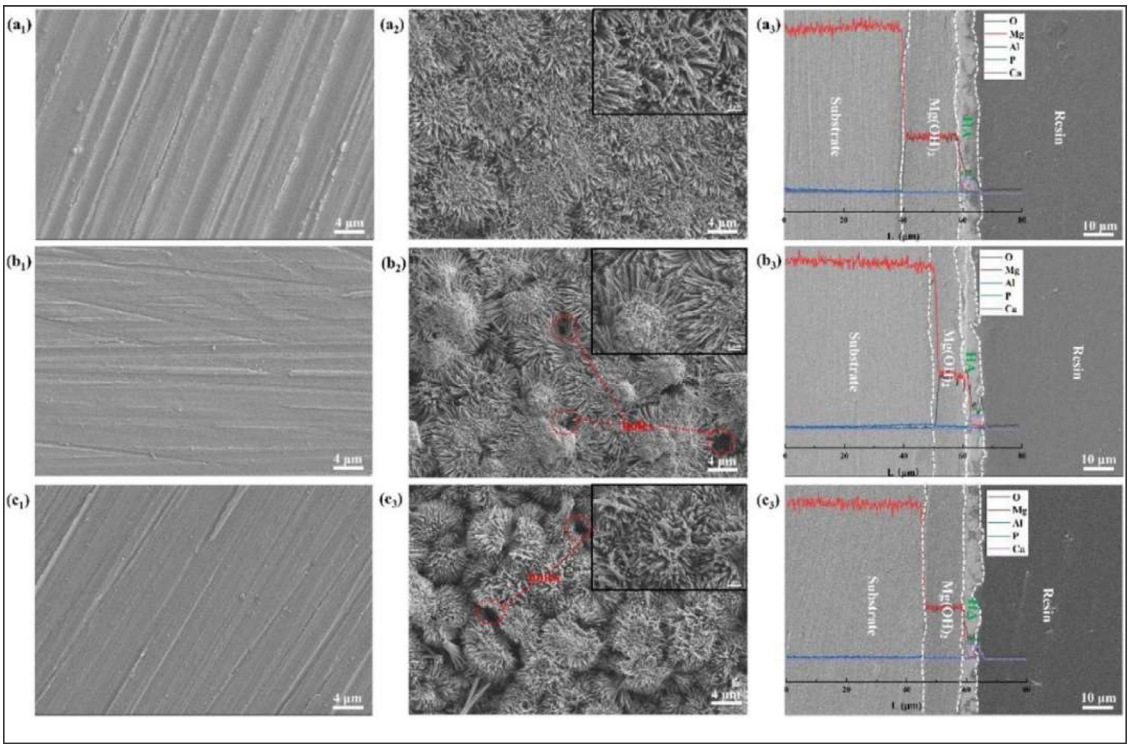

Fig. 9. SEM images of (a_1–c_1) silane-pretreated AZ31 substrates and (a_2–c_2) corresponding HAp/$Mg(OH)_2$-coated samples showing sea urchin-like HA nanostructures. (a_3–c_3) Cross-sectional SEM and EDS line-scan profiles confirming bilayered $Mg(OH)_2$–HAp structure and elemental distribution on HAp/APTES, HAp/GPTMS, and HAp/VTES samples (Reproduced with permission from Ref. [103]. License no: 6050040716452).

On the other hand, apart from chemical functionalization, an innovative physical process, such as femtosecond laser-assisted hydrothermal coating, produced microemulsion cone structures on Mg alloy surfaces that significantly improved HAp nucleation and mechanical interlocking, giving rise to thicker and denser coatings with adhesion strength of ∼31.86 MPa and reduced corrosion rate reaching 0.146 mm/year while stimulating fast osteoblast proliferation [107]. This study showed that HAp coatings significantly improved cell adhesion, and growth compared to surfaces without the coating. The confocal microscopy images with fluorescence staining in Fig. 10 revealed better cell viability and structural organization on HAp-coated surfaces. The CCK-8 proliferation assay results indicated that HAp coatings supported osteoblast growth at different periods. These findings highlight that applying HAp coatings by femtosecond laser-assisted hydrothermal process could work on Mg alloys to support bone formation, making them potential materials for biomedical implants [107].

Further, Zhou et al. have proposed a novel hydrothermal approach using a polydopamine intermediate layer to obtain denser and more uniform HAp coating with good corrosion resistance and cytocompatibility [108]. This chemical approach addresses degradation and bio-integration simultaneously. These investigations signify the development beyond basic HAp deposition toward multifunctional and highly engineered coating systems by hydrothermal process, surface modification, and composite formulations. HAp coatings on Mg alloys developed through the hydrothermal method improve biocompatibility and corrosion resistance. However, they often have low mechanical strength, weak adhesion, and cracking. These problems reduce their durability and effectiveness in load-bearing biomedical implants.

4.3. Biomimetic coating

Simulated Body Fluid (SBF) is an aqueous solution mimicking the ionic composition of human blood plasma. It is mainly used in vitro to test the bioactivity of biomedical materials, especially those proposed for use in bone tissue engineering. The standard SBF contains Na^+, K^+, Ca^{2+}, Mg^{2+}, Cl^-, HCO_3^-, HPO_4^{2-}, and SO_4^{2-} ions within the concentration ranges found in plasma [109]. SBF's primary function is to determine ability of bioactive materials to form bone-like apatite formation on their surfaces under physiological conditions. Several modifications have also been implemented to enhance or modify SBF functionality. Table 5, summarizing different SBF formulations, highlights minor differences in ionic concentrations, with all variants commonly buffered to a physiological pH of 7.4 and at 37 °C incubation. SBF has become a standard preclinical tool in biomaterials research, offering an inexpensive, reproducible approach to screening bioactivity and developing biomimetic coatings [110,111].

Biomimetic deposition is a relatively low-temperature technique inspired by natural bone formation processes [114,115]. Through this process, the Mg alloy is subjected to surface treatment (such as via alkaline treatment or acid etching) to create functional groups or nucleation active sites. These pre-

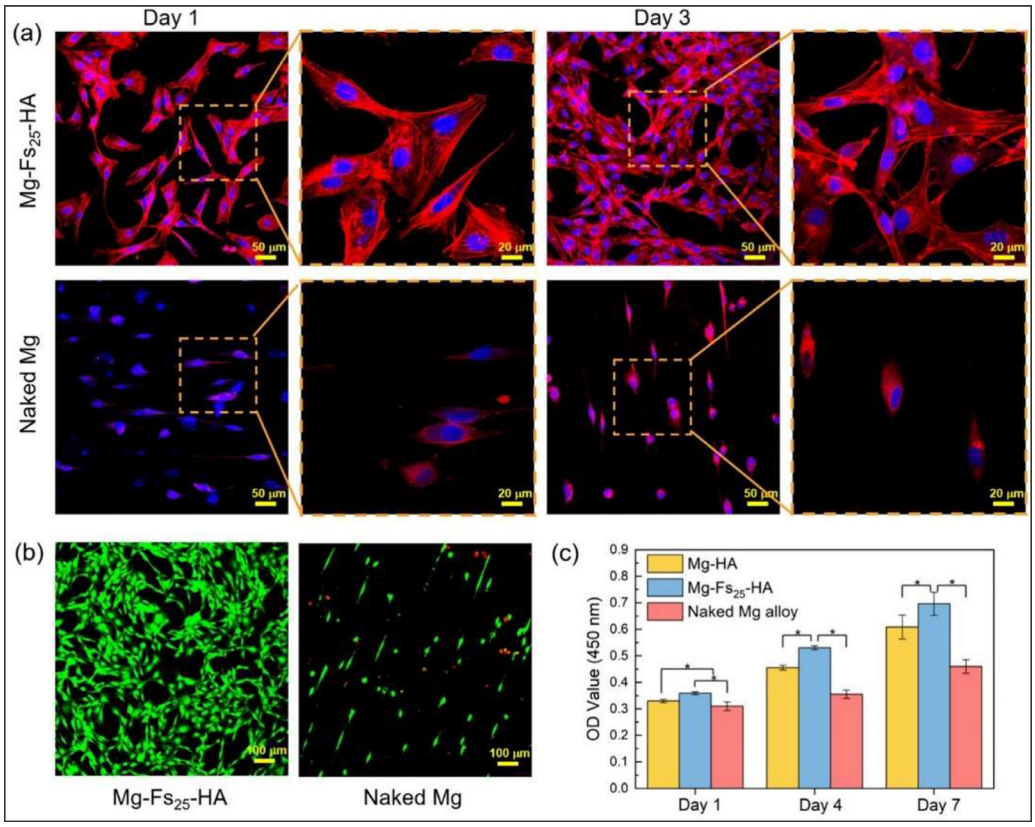

Fig. 10. Cytocompatibility of HAp-coated Mg alloys with MC3T3-E1 cells: (a) CLSM images, (b) fluorescence staining, and (c) CCK-8 assay showing enhanced cell proliferation on HAp-coated samples (Reproduced with permission from Ref. [107]. License no: 6050180469949).

Table 5
Ionic composition of human blood plasma compared with various SBF formulations used for biomimetic HAp coating development [109–114].

SBF type	Ionic concentration (mM)							
	Na^+	K^+	Mg^{2+}	Ca^{2+}	Cl^-	HCO_3^-	HPO_4^{2-}	SO_4^{2-}
Blood plasma	142.0	5.0	1.5	2.5	103.0	27.0	1.0	0.5
Kokubo-SBF	142.0	5.0	1.5	2.5	148.8	4.2	1.0	0
Tas-SBF	142.0	5.0	1.5	2.5	125.0	27.0	1.0	0.5
1.5 × SBF	212.3	7.5	2.3	3.8	186.8	40.5	1.5	0.5
5 × SBF	714.8	0	7.5	12.5	723.8	21.0	5.0	0

treated substrates are dipped in SBF at 37 °C [7,78]. As time progress, Mg reacts with water, forming an $Mg(OH)_2$ layer, and release hydrogen gas as follows.

$$Mg + 2H_2O \rightarrow Mg(OH)_2 + H_2\uparrow$$

This process raises the local pH, thus encouraging the supersaturation of calcium and phosphate ions in SBF. These combine to nucleate and grow as HAp on the surface as follows.

$$10Ca^{2+} + 6PO_4^{3-} + 2OH^- \rightarrow ACP \rightarrow Ca_{10}(PO_4)_6(OH)_2\downarrow$$

Some of the Mg^{2+} ions released from the substrate may enter the HAp lattice and enhance its bioactivity. Fig. 11(a) presents the biomimetic approach to apply HAp coatings on a Mg alloy substrate by immersion into an SBF solution. This low-temperature bioinspired process produces the bone-like apatite coating to enhance corrosion resistance and biocompatibility of Mg alloys. Multiple immersions can yield relatively thicker uniform coatings [115]. Also, biomimetic coatings may contain carbonate substitutions similar to biological apatite. However, coatings induced by SBF are lengthy processing [7,78]. To solve these problems, researchers have looked into functional materials and biomimetic interfaces. These can help to develop uniform nucleation of HAp and improve the integrity of coatings.

Various researchers have investigated different approaches to enhance the biomimetic coating. Gao et al. treated AZ91 Mg alloy with a graphene oxide layer before immersion in SBF to develop a dense and uniform HAp-graphene oxide coating. This coating significantly diminished the corrosion current densities and enhanced electrochemical stability [117]. Another novel technique uses hydrophilic and adhesive hydrogels to enable uniform deposition of HAp. Yang et al. first

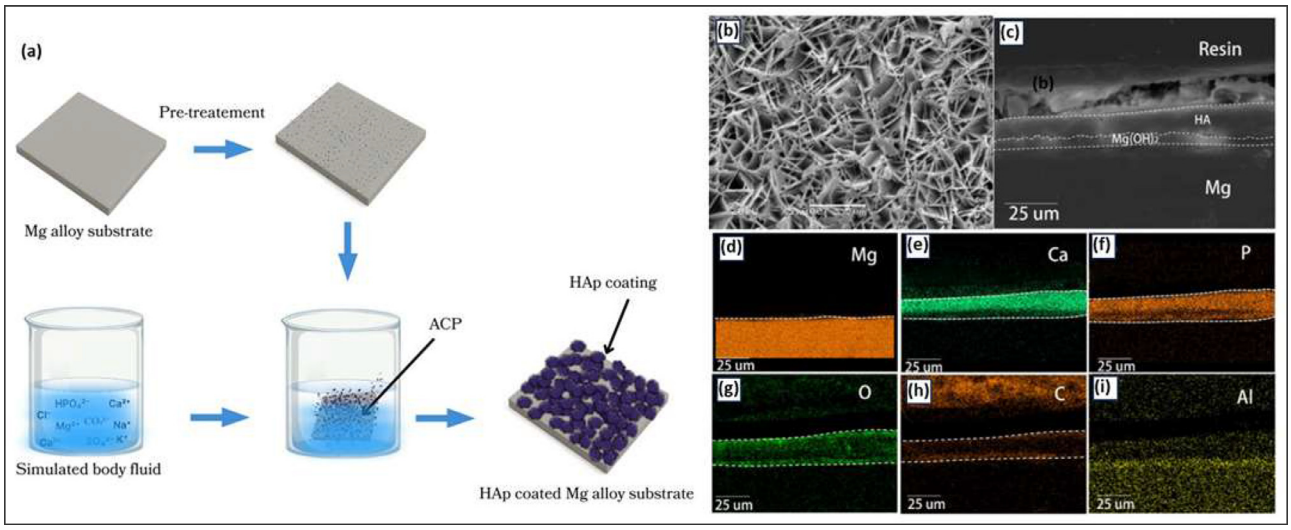

Fig. 11. Schematic illustration of the biomimetic process for fabricating HAp coatings on Mg alloy substrate using SBF. (b) SEM images showing the surface morphology, (c) cross-sectional view, and (d–i) elemental mapping of HAp coating formed by carboxymethyl cellulose-dopamine through the biomimetic method, as reported by Yang et al. Reproduced under Creative Commons license from Ref. [116].

applied a layer of carboxymethyl cellulose-dopamine hydrogel on AZ31 alloy before its immersion in SBF. The hybrid system encouraged dense nucleation of HAp and offered better corrosion resistance. Fig. 11(b–d) shows the surface morphology, cross-sectional view, and elemental mapping of HAp coating formed by carboxymethyl cellulose-dopamine treated substrate through the biomimetic method. Biological studies further showed greater proliferation of MC3T3-E1 osteoblast-like cells, confirming the their potential for use as a biodegradable and bioactive implant coating [116]. Polysaccharide-based systems have also shown promise in supporting biomimetic mineralization. Zhu et al. fabricated a hybrid coating by combining HAp with aminated hydroxyethyl cellulose using a sol–gel spin coating method followed by immersion in SBF [118]. The resulted coating displayed crack-free morphology with improved corrosion resistance, and good biocompatibility. The presence of amine groups in hydroxyethyl cellulose likely enhanced ion exchange and binding, contributing to rapid and stable HAp formation. Lin et al. sprayed AZ31 alloy with a polydopamine film that allowed uniform HAp deposition during subsequent soaking in SBF [119]. The polydopamine-assisted coating showed good electrochemical behavior and enhanced fibroblast cell proliferation. Moreover, researchers have tested biologically active peptides as molecular triggers for apatite nucleation. Cui et al. treated AZ31B alloy with a phosphorylated synthetic peptide resembling phosphophoryn, a bone matrix protein. The peptide suppressed corrosion and thus extensively promoted calcium phosphate mineralization [120]. Other SBF compositions have also been investigated to change the structure and properties of HAp coatings better. Hernández et al. deposited a bilayered HAp coating onto pure Mg using supersaturated calcification solution [121]. The coating were made with a thick inner layer and a porous outer layer, resembling the same hierarchical structure found in bone. In summary, the biomimetic HAp coating approach via SBF is a more physiological and facile way to modify surface features of Mg-based implants. While the basic SBF route can easily form bioactive layers, recent innovations involving carbon-based materials, functional hydrogels, bioadhesives, and biomimetic peptides have contributed significantly to coating stability, corrosion resistance, and biological performance [117–121].

4.4. Electrochemical deposition

Electrochemical deposition consists of passing an electric current to form HAp coating on Mg alloy surfaces from a solution that contains calcium and phosphate ions. It has advantages in terms of coating uniformity and deposition rate. With the different parameters such as voltage, current density, bath composition, pH, and temperature, we can easily tailor the morphology, thickness, and crystallinity of the HAp layer. Cathodic deposition methods are generally used for HAp coating onto Mg substrates [122]. The electrochemical deposition of HAp onto a Mg alloy substrate is shown in Fig. 12(a). The Mg alloy served as the cathode, with the Pt anode immersed in an electrolytic bath containing Ca^{2+} and PO_4^{3-} ions. As the electric current flowed through the circuit, a porous layer of HAp was deposited onto the Mg alloy surface.

The electrodeposition of HAp coatings presents a series of electrochemical processes leading to a biocompatible coating [122]. When a constant potential or current is applied, the cathode, which is the surface of the Mg alloy, reduces water. This process releases OH^- ions and produces hydrogen gas through the following reaction.

$$2H_2O + 2e^- \rightarrow H_2(g) + 2OH^-$$

This reaction increases the pH near the cathode, creating an alkaline environment that favors the supersaturation of Ca^{2+}

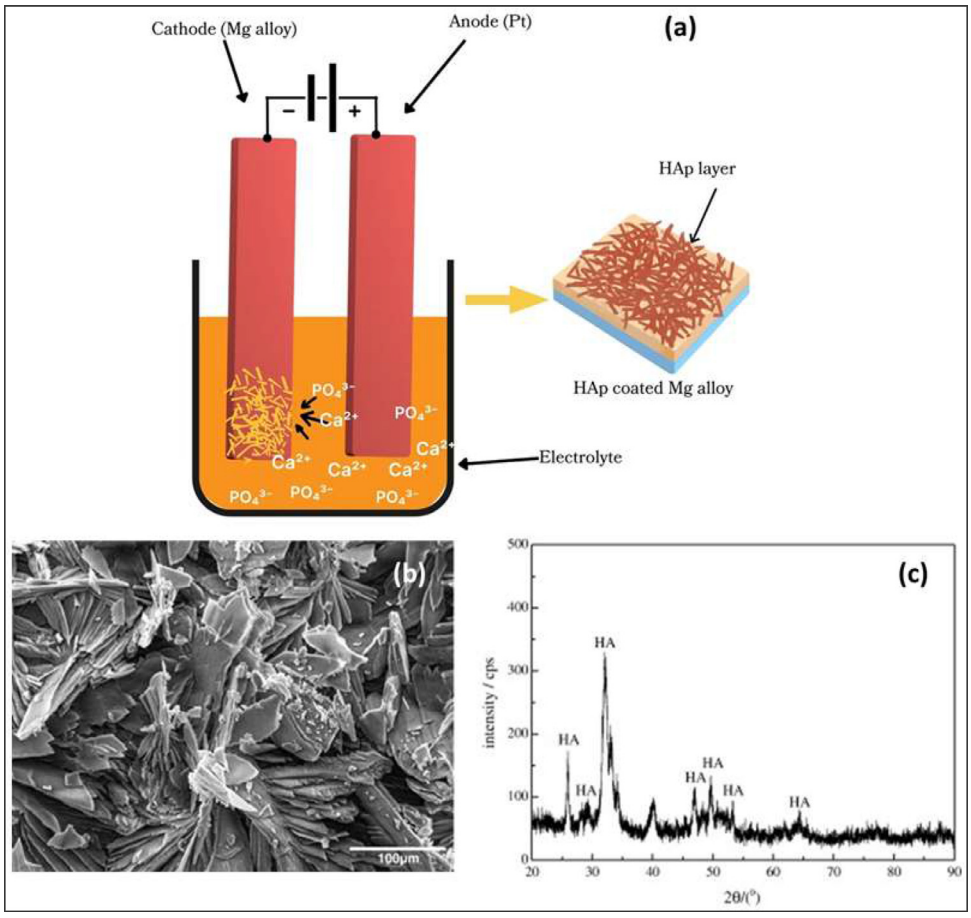

Fig. 12. (a) Schematic illustration of a typical electrochemical deposition process of HAp on a Mg alloy. (b) SEM image revealed surface morphology and (c) XRD pattern of the HAp coating on AZ91D Mg alloy, as reported by Song et al. (Reproduced with permission from Ref. [123], License no: 6104630455801).

and PO_4^{3-} ions in the electrolyte. These ions are usually contributed from salts such as calcium nitrate ($Ca(NO_3)_2$) and ammonium phosphate ($(NH_4)_2HPO_4$), where association of ionic calcium and phosphate ions initiates the formation of some intermediate calcium phosphate phases [124,125]. During deposition, these intermediates convert into HAp crystals with the following overall reaction:

$$10Ca^{2+} + 6PO_4^{3-} + 2OH^- \rightarrow Ca_{10}(PO_4)_6(OH)_2 \downarrow$$

Now, HAp nucleates and grows on the Mg alloy surface as a dense and adherent coating. At the same time, the Mg substrate could be partially dissolved, releasing Mg ions:

$$Mg \rightarrow Mg^{2+} + 2e^-$$

Mg ions can enter the HAp lattice, potentially changing its crystallinity or bioactivity [124,125]. Since this is a chemical deposition, it depends on several parameters such as electrolyte concentration, temperature, voltage or current applied, and deposition time. These parameters can affect the morphology of the coating, its thickness, and the characteristics of HAp deposits. The adhesion strength of the coatings formed by electrochemical deposition can be improved further by pulse or alternating current deposition processes that can improve the microstructure of the coatings and the bonding strength at the interface. Electrochemical methods are scalable and inexpensive, offering an additional advantage toward industrialization of this coating method [124,125].

According to several studies, electroplated HAp coatings help to increase corrosion resistance. For example, calcium phosphate coatings were applied by Jamesh et al. onto Mg substrates, starting with the formation of DCPD [126]. Immersion of the coatings in an alkaline solution converted DCPD to crystalline HAp. The coating provided about a threefold increase in corrosion resistance in SBF, emphasizing the importance of post-treatment on phase purity and stability of the coating. Song et al. reported that electrochemical HAp coatings on AZ91D Mg alloy with flake-like structure (Fig. 12) with reduced the corrosion rate in physiological environment [123]. Recent electrodeposition developments have also focused on controlling the chemical composition of the coating to provide better performance. HAp with dopants such as copper, fluorine, and strontium can provide antimicrobial properties, corrosion resistance, and differing effects on biological response. The ultrasonic-assisted pulse-reverse electrodeposition of copper-doped fluoroHAp (Cu-FHAp) on AZ31 Mg alloy has been studied by Akbarpour et al., in which uniform copper incorporation into the coating matrix was achieved

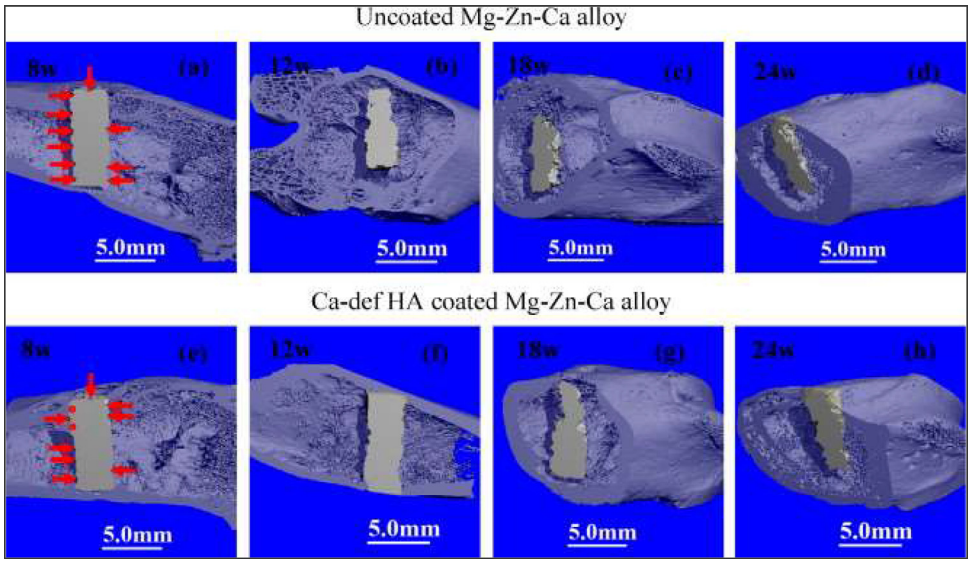

Fig. 13. 2D micro-CT images showing femora with Mg implants (Reproduced with permission from Ref. [130]. License no. 6050190265467).

[127]. The doped coatings provide a superhydrophobic nature onto the surface with contact angles of approximately 136°, with good in vitro corrosion-resistant ability. Cytotoxicity assays revealed the coatings to be biocompatible, indicating that copper doping may offer multifunctional benefits by combining corrosion resistance and antimicrobial properties. Surface morphology and wettability also directly affect coating performance. Meng et al. investigated pulsed electrodeposition of fluorine-doped HAp (FHAp) with hydrogen peroxide additives to develop dense rod-like FHAp coatings on Mg-Zn-Ca alloy with better corrosion resistance than continuous deposition [128]. This study revealed that the enhanced bioactivity imparted by FHAp would enable apatite formation, almost simulating natural bone mineralization [128]. Wang et al. developed a Ca-deficient HAp coating on Mg-Zn-Ca alloy using pulsed electrodeposition[129]. They found that the coating slow down the in vivo degradation of the alloy and enhanced its bone response. The micro-CT images (Fig. 13) showed that bare Mg implants had severe corrosion with deep pits as early as 8 weeks. In contrast, those with Ca-deficient HAp coating showed slight superficial corrosion in the early phase. With increasing implantation time, coating degradation induced localized corrosion, but still less than that of bare Mg. These results indicates that Ca-deficient HAp coatings slow down the in vivo degradation and holding an excellent potential for Mg-based orthopedic implants [130].

Post-deposition surface treatments also contribute significantly to coating adhesion and corrosion resistance. Chen et al. treated phytic acid, a natural chelating agent, to modify electrodeposited HAp coatings on AZ31 Mg alloy [131]. Phytic acid enhanced coating-substrate chemical bonding while increasing coating compactness and mechanical strength. The best phytic acid concentration (8 g/L) produced an adhesion strength of 10.32 MPa and a 0.46 mm/year corrosion rate in Hank's solution. Wang et al. found that calcium-deficient HAp forms very fast during pulse electrodeposition on Mg-Zn-Ca alloys, while its crystallinity increases over time when governing conditions of pH and temperature favor HAp precipitation [129]. The study further revealed that Mg^{2+} ions released from the substrate can partially substitute for calcium sites in the HAp lattice, affecting crystallinity and biological behavior. Therefore, electrochemical deposition is the most promising technique for producing bioactive and corrosion-resistant HAp coatings onto Mg alloys for biodegradability-related implant applications. Further functionality improvements come from including dopants into the materials, developing superhydrophobic surfaces, and using environmentally friendly surface modifiers.

4.5. Electrophoretic deposition

One of the most commonly used methods for depositing HAp coatings on Mg alloy substrates is electrophoretic deposition (EPD), which creates a smooth surface layer, well-attached and bioactive, thus enhancing corrosion resistance and biocompatibility [133]. The process begins with preparing a stable suspension composed of charged HAp particles dispersed in an appropriate solvent such as ethanol or water. Stability of the colloidal suspension is essential and may be attained by adjusting the suspension's pH and dispersing agents. When a DC electric field is applied across the suspension between two electrodes, the charged particles migrate electrophoretically towards the oppositely charged electrode [132,133]. The Mg alloy substrate usually works as the cathode (negatively charged), so it attracts the positively charged HAp particles as shown in Fig. 14(a). The electrophoretic velocity (v) of the particles can be expressed as per the smoluchowski equation [134]:

$$v = (\varepsilon\zeta/\eta)E$$

where ε is the dielectric constant of the medium, ζ is the zeta potential or charge on the particle surface, η is the viscosity of the suspension, and E is the applied electric field strength. As the particles moved and accumulated on the surface of

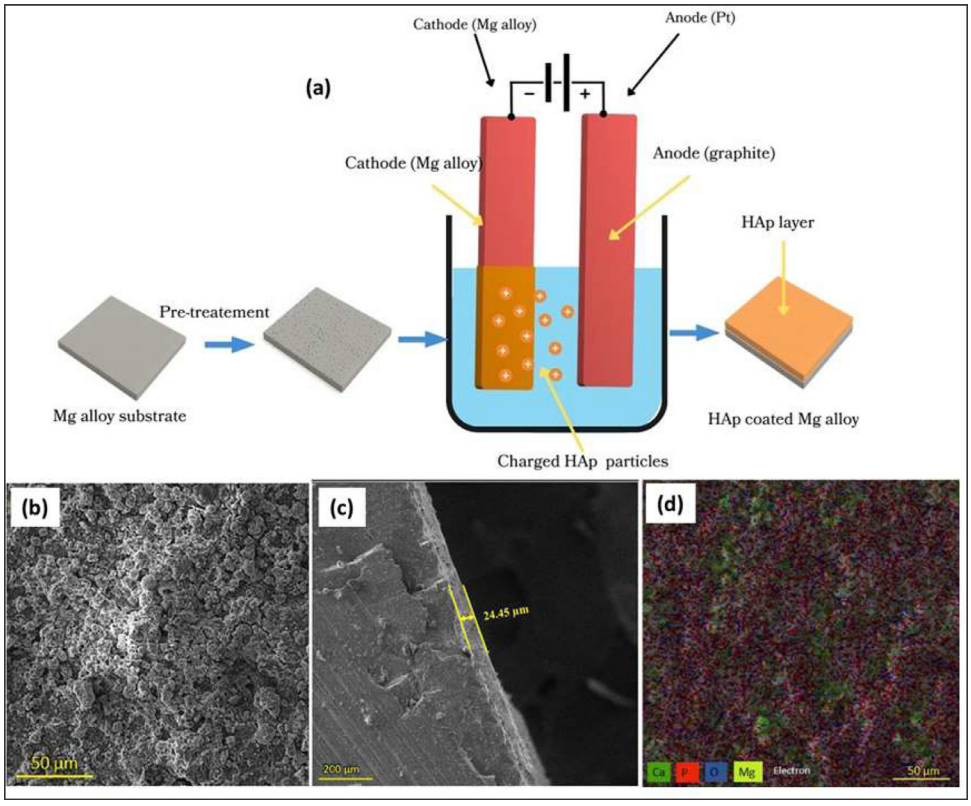

Fig. 14. (a) Schematic representation of the electrophoretic deposition of HAp on a Mg alloy substrate. (b–d) SEM micrographs with elemental mapping showing the HAp coating on the Mg substrate reported by Akram et al. (Reproduced with permission from Ref. [132]. License no: 6143550384207).

Mg, the coating formed a coherent and dense HAp coating layer. The deposited mass m is modeled by Hamaker's relation [135]:

$$m = C\,\mu\,E\,t$$

where C is the particle concentration in the suspension, μ is the electrophoretic mobility ($\mu = v/E$), E is the electric field, and t is the deposition time. To achieve the best coating thickness, density, and uniformity, it is necessary to monitor process parameters closely. These include voltage, deposition time, suspension concentration, and pH. After deposition, the coatings are dried and usually annealed with low heat to improve crystallinity and bonding to the Mg substrate. During heat treatment, the temperature must be low enough to prevent oxidation or damage to the Mg alloy. EPD is favored for its simplicity, low processing temperature, ability to coat complex shapes, and precise control over coating parameters, making it highly suitable for biomedical implant surface modification [7,133].

Akram et al. reported an approach to optimize the EPD parameters when coating pure Mg with HAp nanoparticles (Fig. 14(b–d)) to improve surface hydrophilicity, mechanical stability, corrosion resistance, and osteoconductive potential during long-term immersion in SBF [132]. This study showed that the EPD coating could remarkably slow the degradation rate and improve biological performance, and suggested that EPD could practically become the scalable route toward reliable biodegradable implants. Rojaee et al. demonstrated found that MAO pretreatment on AZ91 Mg alloy, followed by electrophoretic deposition of nanostructured sol–gel HAp coating offer better corrosion resistance and apatite formation in SBF [89]. In another study, Kumar et al. demonstrated that smoother Mg-3Zn-alloy substrates yielded uniform and crack-free coating by EPD and annealed HAp coatings to enhance corrosion resistance by about 25 times and enhanced osteogenic cells adhesion. This study indicates the surface treatment followed by heat treatment can influence both mechanical integrity and biological response of the coating [136]. Aver et al. investigated the comparative coating performance of synthetic shell and natural shell waste-derived HAp coating on AZ31 Mg alloy and found that nano-HAp derived from ostrich eggshell exhibits the highest adhesion strength and corrosion resistance [137]. Furthermore, Tayyaba et al. studied the effect of coating thickness and durability on corrosion resistance HAp coating [138]. This coating dropped the anodic current density by one order of magnitude. At the same time, the reduction in corrosion rate was more than fivefold compared with bare Mg. This study clearly indicates coating thickness and microstructural integrity as key parameters controlling the degradation of the implant.

Composite materials combining HAp with fluorides, bioglass, chitosan, and graphene oxide have been explored to improve the multifunctionality of coatings further. Rojaee et al.

reported that the FHAp coatings, having 25% fluorine substitution and deposited on micro-arc oxidized AZ91 Mg alloy, increased corrosion resistance and induced bioactivity and bone ingrowth while minimizing Mg degradation rates during in vitro tests [139]. Therefore, fluoridation serves as an efficient method for tuning biodegradability versus biofunctionality. Conversely, Singh et al. created multifunctional nanocomposite coatings, including HAp, bioglass, chitosan, and magnetite (Fe_3O_4) nanoparticles, onto AZ91 Mg alloy by EPD. Presence of Fe_3O_4 enhanced corrosion protection and hemocompatibility, with hemolysis rates lower than 5%, which suggests the hybrid coatings resist degradation while simultaneously ensuring blood compatibility [140]. According to Saadati et al., an additional amount of 1 wt% graphene oxide, accompanied by a controlled voltage during electrophoretic deposition, would yield dense and uniform coatings exhibiting good adhesion and corrosion resistance on a complex Mg alloy, where graphene oxide acts as an enhancer of the barrier properties of coatings and durability of implants [141]. Hence, the electrophoretic deposition of HAp and its composites on Mg alloys can be a potential key to solving the rapid degradation and biocompatibility issues faced by Mg-based biodegradable implants. EPD coatings with optimized process parameters, surface pretreatment, and improved materials, such as the addition of natural biowaste sources and multifunctional nanocomposites, offer enhanced corrosion resistance along with good mechanical integrity and biological performance.

4.6. Plasma electrolytic oxidation

Plasma electrolytic oxidation (PEO), also called micro-arc oxidation (MAO), is the most advanced surface treatment technique to produce thick, dense, and strongly adhering HAp coatings on Mg alloy substrates [142–144]. An oxide-based ceramic layer is formed through high-voltage anodic oxidation of the specimen in an electrolyte containing calcium and phosphate ions. When the voltage is sufficiently high (300 $\sim$ 600 V), the dielectric breakdown can occur at the metal-electrolyte interface, resulting in local micro-arc discharges or plasma sparks [142–144]. These sparks create extremely high temperatures, which favor the formation of the crystalline HAp and other oxide phases in situ on Mg alloy surfaces. The basic electrochemical reaction of Mg oxidation during MAO can be expressed as follows:

$$Mg \rightarrow Mg^{2+} + 2e^{-}$$

These electrons reduce water molecules in the electrolyte to produce hydroxide ions and hydrogen gas:

$$2H_2O + 2e^{-} \rightarrow H_2 + 2OH^{-}$$

The Mg ions react with hydroxide ions to form $Mg(OH)_2$:

$$Mg^{2+} + 2OH^{-} \rightarrow Mg(OH)_2$$

The electrolyte carries Ca^{2+} and PO_4^{3-} ions that can combined under plasma conditions to produce HAp as follows:

$$10Ca^{2+} + 6PO_4^{3-} + 2OH^{-} \rightarrow Ca_{10}(PO_4)_6(OH)_2 \downarrow$$

The combination of high temperature and energetic plasma discharges leads to the quick crystallization of HAp and its good adherence to the Mg substrate. Parameters such as applied voltage, current density, electrolyte composition, and processing time can affect the formation of the oxide coating [142,143]. Based on corrosion resistance and bioactivity requirements, the thickness and porosity of the MAO coating may be altered by changing the above key parameters. Otherwise, the MAO coating is usually mixed in phases, e.g., MgO, magnesium phosphate, and crystalline HAp phases. The MAO process has numerous advantages over traditional coatings such as an excellent bond strength due to metallurgical bonding, improved corrosion and wear resistance, ability to coat complex geometries, etc.. This process need aqueous electrolytes and does not involve toxic precursors or solvents [145–147].

Despite its benefits, the MAO method also has its drawbacks. The coatings' surface roughness is generally higher than that produced by PVD or sputtering. In addition, the porosity in MAO coatings, while great for cell attachment, also becomes a path to corrosion if the coating is not thick enough. We can modify the thickness, roughness, porosity, and bioactivity by setting key parameters such as current density, electrolyte composition, and processing time. However, the challenge is to resolve corrosion protection versus biological performance with MAO due to its porosity and surface roughness. Gnedenkov et al. used PEO to obtain deposited HAp coatings on Mg-0.8Ca alloy, demonstrated a uniform distribution of calcium, phosphorus, and oxygen throughout the thickness of the coating [148]. Fig. 15 illustrates the cross-section with SEM and EDX elemental mapping, revealing that a uniform HAp coating has been formed over the surface of Mg-0.8Ca alloy. This uniformity was essential to delay corrosion onset and ensure the controlled biodegradation of implants. Further, Usmaniya et al. fabricated an organic–inorganic hybrid system by depositing a chitosan loaded with HAp and bioactive glass particles onto PEO-treated ZM21 Mg alloy [149]. The composite coating exhibit less corrosion current density of five orders of magnitude (from 1.07×10^{-5} to 4.56×10^{-10} mA/cm²) due to the dense barrier effect and bioactive nature offered by the bioactive glass-HAp matrix. Furthermore, the coating favored apatite formation and showed excellent in vitro cytocompatibility. Keyvani et al. have systematically studied the loading of HAp nanoparticles by PEO coating on AZ31 Mg alloy with different concentrations of HAp (1, 3, and 5 g/L) [150]. The result indicates that a concentration of 3 g/L was best for performance with the thickest coating ($\sim$22.5 μm), the smallest average pore size ($\sim$8.7 μm), and the lowest corrosion current density (0.034 μA/cm). Chaharmahali et al. also studied HAp–PEO coatings on AZ31B alloy to determine the effect of increasing HAp concentration in the electrolyte. This study demonstrates

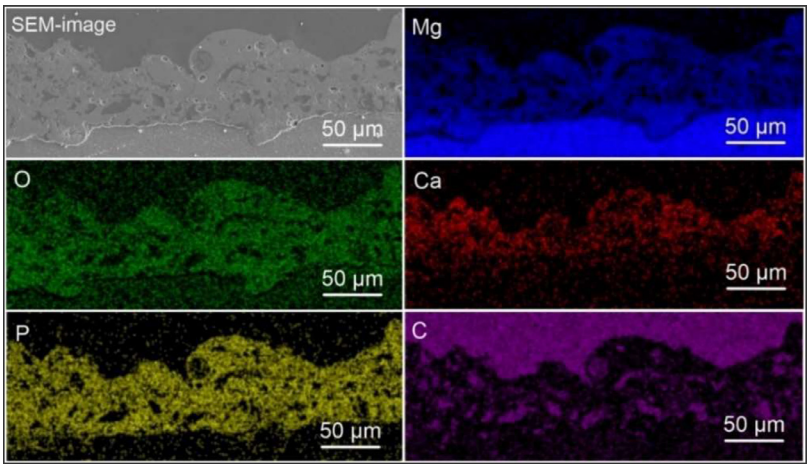

Fig. 15. SEM cross-section and EDX maps confirming the homogeneous formation of HAp coating on Mg-0.8Ca alloy. Reproduced under Creative Commons license from Ref. [148].

increased coating thickness and decreased porosity with an increasing HAp concentration from 5 to 15 g/L, conferring improved corrosion protection in SBF [151]. Moreover, Liu et al. investigated a novel approach in which a self-sealing HAp-MgO composite coating was applied to AZ31 via a one-step MAO process by adding HAp nanoparticles into the base electrolyte. Interestingly, the HAp particles preferentially accumulated in the outer porous layer and sealed the surface micro-defects effectively, while the inner barrier layer was mainly composed of MgO. Such a distribution was favorable in providing corrosion resistance in Hank's solution [152]. Then, moving further toward multifunctional coatings, Momeni et al. optimized the PEO process to co-deposit HAp and silicon dioxide (SiO_2) nanoparticles onto AZ31 Mg alloy [153]. The composite coating showed significantly reduced porosity (~10.3%) and thicker coating layers. EIS studies showed stable corrosion resistance for 7 days of storage in SBF. More importantly, the SiO_2-HAp dual composition promoted much better HAp nucleation and bioactivity than the single SiO_2 coating. Similarly, Gao et al. created HAp-magnesia coatings on Mg using plasma electrolytic oxidation (PEO) and then cathodic electrodeposition (CED) [142]. The SEM surface images (Fig. 16 (a and c)) and cross-sectional images (Fig. 16 (b and d)) show that the PEO layer develops a porous barrier with cracks. The HAp layer deposited through CED fills these pores, forming a denser, uniform protective layer. The potentiodynamic polarization curves in Fig. 16(e) show that bare Mg has the highest corrosion current density. The PEO coating increases corrosion resistance, while the combined PEO+CED coating offers the best protection, demonstrating a more positive corrosion potential and a lower current density. Therefore, MAO/PEO remains an effective and flexible platform for designing bioactive and corrosion-resistant coatings on Mg alloys. However, further optimization is needed to balance the properties of coating roughness, porosity, mechanical integrity, and degradation kinetics, primarily in the applications of load-bearing and biodegradable implants.

4.7. RF magnetron sputtering

The RF magnetron sputtering is a widely accepted physical method for depositing HAp coatings onto biodegradable Mg alloys [156]. In this method, an alternating radio frequency voltage, usually around 13.56 MHz, is applied to the HAp target, leading to the plasma discharge formation in the low-pressure argon atmosphere. The inert argon gas is ionized into positively charged argon ions (Ar^+), which, being accelerated toward the negatively biased HAp target, sputter off atoms or clusters of HAp from the target surface. The sputtered atoms or clusters are then carried through the vacuum chamber and deposited onto the alloy substrate, forming a thin and uniform HAp coating [156–158]. Fig. 17(a) illustrates the schematic of a typical RF magnetron sputtering system. This "magnetron" arrangement takes advantage of the magnetic field near the target surface to trap electrons and thus maintain a high ionization efficiency, leading to an enhanced sputtering rate and providing lower substrate heating. Basic sputtering process given by the reaction [156–158]:

$$Ar\ (gas) \rightarrow Ar^+ + e^-\ (in\ plasma)$$

$$Ar^+ + HAp\ (target) \rightarrow HAp^0\ (neutral\ atoms/clusters) + Ar\ (reflected)$$

$$HAp^0\ (vapor\ phase) \rightarrow HAp\ (solid\ film\ on\ substrate)$$

The film thickness, crystallinity, adhesion strength, and biological performance of HAp coating depend on parameters such as RF power, working pressure, substrate bias, deposition time, and substrate temperature. Post-deposition annealing is often used to enhance the crystallinity of HAp coating. Fig. 17(b) revealed the morphological feature of the HAp-coated AZ31 alloy prepared by the RF sputtering process.

The RF magnetron sputtering of HAp coatings is found helpful in improving the corrosion resistance and biofunc-

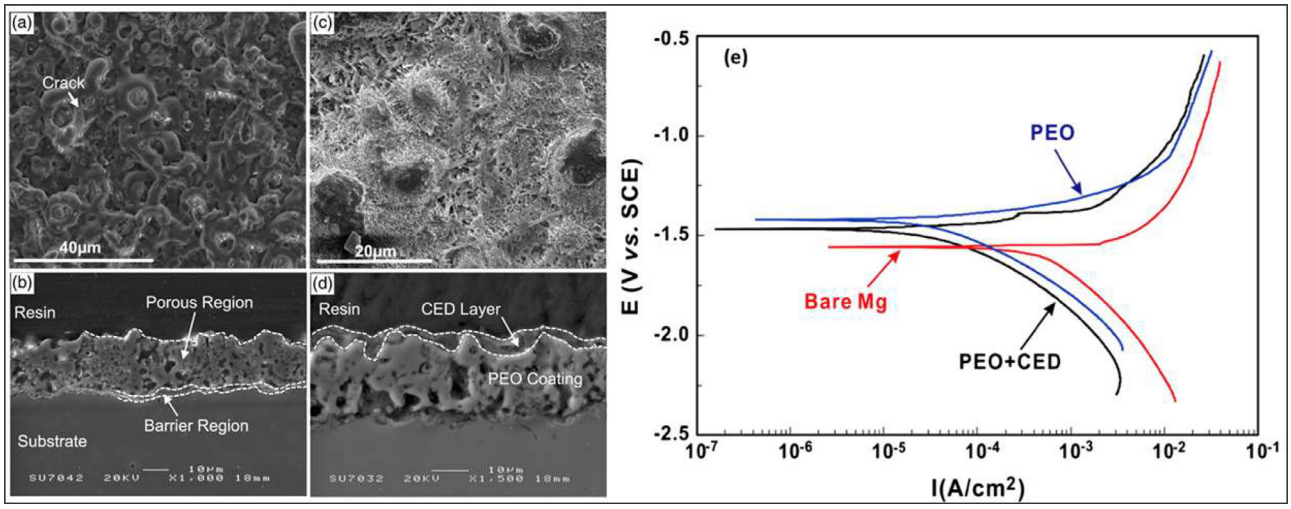

Fig. 16. Surface and cross-sectional morphologies of PEO coatings without (a, b) and with (c, d) CED HAp layers. (e) Potentiodynamic polarization curves of the corresponding samples in SBF (Reproduced with permission from Ref. [142]. License no.: 6106350757634).

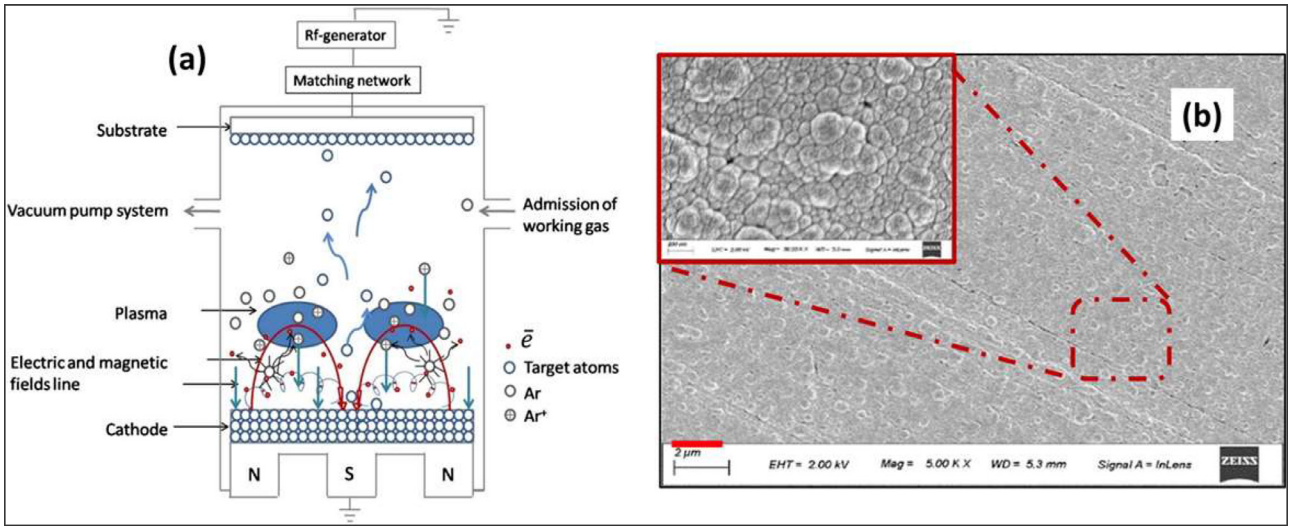

Fig. 17. (a) Schematic representation of a typical RF magnetron sputtering system (Reproduced with permission from Ref. [154], License no: 6050071430938). (b) SEM image of the HAp-coated AZ31 alloy prepared by the RF sputtering process, as reported by Yadav et al. (Reproduced with permission from Ref. [155], License no: 6104640331006).

tionality of biodegradable Mg alloys in physiological environments [156,157]. For example, Surmeneva et al. deposited ultrathin HAp films with 550 to 750 nm thickness in Mg-Ca alloys and observed degradation behavior in vitro in SBF [159]. The electrochemical tests revealed that coating with HAp increased the resistance to polarization by more than two orders of magnitude and lowered the corrosion current density by almost 98% compared to uncoated alloys, indicating the effectiveness of the coating as a barrier of protection. Similarly, Mukhametkaliyev et al. also reported improved corrosion resistance for nanostructured HAp-coated films applied by RF sputtering onto AZ91 Mg alloys [160]. Further, corrosion tests indicated that after 7 days, the uncoated alloy had almost seven times the rate of weight loss compared to the coated alloy. The SEM images after electrochemical corrosion testing (Fig. 18) further supported these conclusions, wherein the bare AZ91 alloy exhibited many deep corrosion pits and widespread localized attack, while the HAp-coated surface remained intact with only minor surface corrosion. Thus, applying nanostructured HAp coating significantly enhanced the corrosion resistance and long-term durability of the AZ91 Mg alloy in physiological environments.

Working on the clinical significance, Dragomir et al. studied the HAp coatings on the Mg-Zn-Ag alloys deposited at 300 °C to improve the performance of implants in orthopedic trauma applications [161]. The higher deposition temperature allowed the formation of crystalline HAp with nearly stoichiometric calcium-to-phosphorus ratios. The electrochemical tests at physiological conditions eventually revealed higher corrosion resistance, while mechanical investigations confirmed coating adhesion and uniformity on differ-

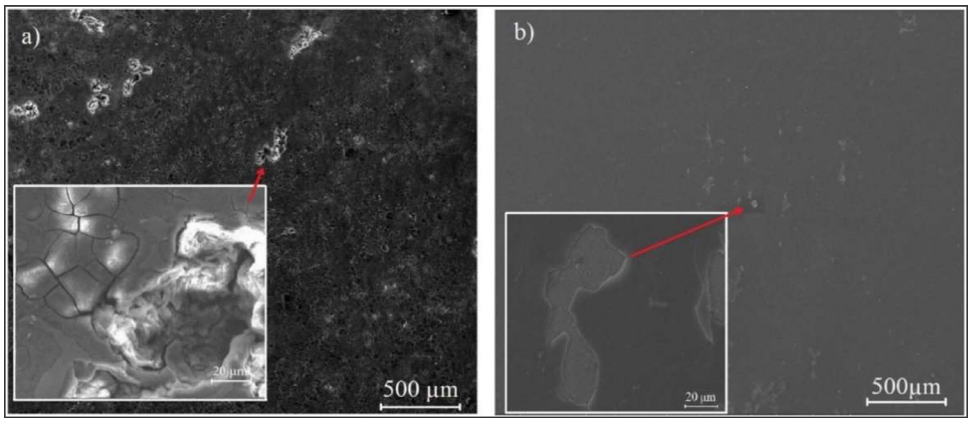

Fig. 18. SEM images of uncoated (a) and HAp-coated (b) AZ91 Mg alloys, illustrating the corroded surface morphology (Reproduced with permission from Ref. [160]. License no: 6050171154800).

ent alloy compositions. Controlling the deposition temperature is a key parameter governing the microstructure and properties of the coating. In a systematic study, Parau et al. varied the deposition temperature for HAp coatings on AZ31B Mg alloy from room temperature to 400 °C [162]. The analyses revealed that grain growth increases with temperature, and a slight decrease in hardness occurs. The coating deposited at 200 °C providing nearly ∼97.3% of protection against corrosion owing to the least porosity among all other coating. All coatings obtained above this temperature showed less mechanical strength and corrosion resistance, putting forward 200 °C as the optimum deposition temperature for biomedical implant coatings. Further, Pana et al. have shown that doping HAp coating with Mg and deposition at 200 °C could improve mechanical hardness, elastic modulus, and resistance to corrosion on AZ31B alloys [163]. To get a corrosion-resistant, mechanically stable, and biologically performing coating, a fine balance should be maintained between the process parameters such as deposition temperature, target doping, and so on. Table 6 presents an overview of sol-gel, hydrothermal, biomimetic, electrodeposition, electrophoretic deposition, micro arc oxidation, and RF sputtering methods used for HAp coating on Mg-based biomaterials. The comparison addresses processing conditions, technical advantages, and present challenges.

5. Advancement in HAp-based coating on Mg alloy to improve the performance

Nanostructuring, ion substitution, hybridization, smart responsiveness, drug delivery, and bioinspired multifunctionality have directed HAp coatings on Mg alloys into tailored systems. These modifications are made to increase corrosion resistance and mechanical strength. They can also provide antibacterial protection, induce bone growth, and dynamic adaptability for next-generation biodegradable orthopedic implants [1,7,164,165]. The first approach is engineering nanostructured HAp coatings through innovation in coating methodologies. Nanoscale coatings at the morphological and crystallographic level closely resemble natural bone minerals, showing enhanced compatibility with biological tissues [166]. Further, this nanoscale morphology can be utilized to control the degradation rate and complete the healing of bone [61]. Advanced methodologies for HAp coating on Mg alloys include the simultaneous use of more than one technique to optimize the coating performance in corrosion resistance, adhesion, and bioactivity, and provide multifunctionality. Microwave-assisted synthesis yields fast and uniform crystallization, while ultrasonication helps in the dispersion of particles and better bonding. Such advances help bring about durable, functional, and tailor-made coatings suitable for osteogenesis and extension of implant life. Shen et al. fabricated FHAp coatings with hierarchical micro/nano-topography mimicking natural bone resorption surfaces on Mg alloy via microwave aqueous method [167]. They revealed that the surface morphology of the HAp and FHAp coatings has distinct nanostructures. HAp-coated samples showed nanocotton and nanosheet features (Fig. 19a–d) while FHAp-coated samples formed dense nanoneedles (Fig. 19e–h). Elemental analysis showed that calcium, phosphorus, and fluorine were distributed homogeneously in FHAp nanoneedles (Fig. 19i). 3D optical profiling and roughness analysis further revealed that the FHAp coating had significantly higher surface roughness and peak spacing than the HAp coating, suggesting an improved surface texture (Fig. 19j–l). Such bilayer nanoneedle arrays promoted osteogenesis and showed outstanding anticorrosion performance in SBF and fast osseointegration.

Concerning the surface morphology, Sun et al. used an ultrasonic aqueous synthesis method to fabricate dense and crack-free HAp coatings with a bamboo leaf-like microstructure on Mg substrates [168]. Within 1 h of ultrasonic cavitation in calcium-phosphate solutions, a relatively uniform layer was formed, and strong interfacial bonding of about 18.1 ± 2.2 MPa was achieved. Electrochemical results in SBF proved good corrosion resistance, while the rapid deposition of apatite within 3 days showed the coating was highly bioactive. The coating continued mineralizing for 90 days, thus indicating its long-term protective capacity and biocompatibility for orthopedic applications. Complimentary to this approach,

Table 6
A comparative representation of selected methods for HAp coatings on biodegradable Mg alloys with respect to their principles, processing conditions, advantages, and limitations.

Method	Principle	Processing conditions	Advantages	Limitations
Sol–gel	Hydrolysis and condensation of precursors to form HAp gel	Low-temp drying and calcination (∼<600 °C)	Low cost, uniform coatings, compositional control	Requires heat treatment, may produce cracks due to shrinkage
Hydrothermal	Crystallization of HAp in aqueous solution under high temp/pressure	120–200 °C, autoclave, hours to days	Good crystallinity, strong adhesion, dense coatings	Long processing time, specialized equipment
Biomimetic	HAp growth in SBF mimicking natural mineralization	Room to body temp, immersion for several days	Excellent bioactivity, low cost, environmentally friendly	Slow coating rate, thin coatings, may need surface pre-treatment
Electrodeposition	Electrochemical reduction to deposit HAp from ionic solution	Room temp, 1–24 V, aqueous electrolyte	Simple setup, good control over thickness and morphology	Requires post-treatment for densification, risk of porosity
Electrophoretic Deposition (EPD)	HAp particles are deposited from suspension via electric field	Room temp, organic/aqueous media, DC/AC field	Uniform coating, fast deposition, simple equipment	Requires sintering, weak adhesion without an interlayer
Micro Arc Oxidation (MAO)	Plasma-assisted formation of oxide/ceramic layer on Mg substrate	High voltage (200–500 V), electrolyte bath	Strongly adherent layer, porous structure enhances HAp bonding	Brittle layer, risk of cracks, rough surface
RF Sputtering	HAp target is sputtered onto Mg surface using radio frequency plasma	High vacuum, substrate heating (∼300–600 °C)	Dense, uniform films, good adhesion, high purity	Expensive equipment, low deposition rate, high residual stress

Wang et al. developed a double-layer coating comprising microarc oxidation followed by fluoridated HAp (FHAp) deposition on Mg-3Zn-0.5Zr-0.5Sr alloy [169]. The microarc oxidation acted as a base-layer from a corrosion resistance viewpoint, whereas the needle-shaped FHAp layer (∼6 μm thick) offers osteoconductivity and mineralization ability and hence stands as a potential coating material for improvement of Mg implants performance.

Ionic-substituted HAp coatings are recently considered for enhancing biological functionality. Such coatings containing Mg^{2+}, Zn^{2+}, Sr^{2+}, Si^{4+}, and CO_3^{2-} ions can facilitate osteogenesis, angiogenesis, and antimicrobial activities without affecting the structural integrity of HAp. These substitutions also affect solubility and degradation behavior, making the coating better suited to Mg alloys. Such coatings provide a multifunctional surface that supports bone regeneration, lowers infection risk, and controls biodegradation. Sr-doped HAp coatings were prepared on a ZK60 Mg alloy via one-pot hydrothermal synthesis by Wang et al., who found that 10% Sr substitution changed the morphology from nanorods to a 3D nanowire network, thereby improving corrosion resistance and assisting in better adhesion and proliferation of BMSCs [170]. Fig. 20 revealed the growth mechanism and SEM images of Sr-HAp coatings on ZK60 Mg alloy. This Sr substitution modified the coating structure, osteointegration, and biodegradation behavior, thus making it more applicable for orthopedic applications. Also, Sr-substituted HAp coating on Mg alloy were found to have an excellent corrosion resistance. Hydrogen evolution was much less for Sr-substituted HAp-coated alloys than for non-coated ones, thus reducing corrosion [171]. The pH of the Hank's solution was much more stable with Sr-substituted HAp-coated alloys suggesting that coating prevents localized acidification. Fig. 21 clearly shows the effect of Sr substitution on hydrogen evolution, pH change, Mg release, and corrosion rates of Sr-HAp-coated Mg alloys in Hank's solution. The above results show that Sr-HAp coatings, especially those with 100% Sr content, afforded the best corrosion protection, highlighting the potential of Sr-HAp coating for developing Mg alloys in biomedical areas.

Similarly, Zhou et al. showed that Zn-doped nanowhisker HAp coatings hydrothermally synthesized on ZK60 alloy enhanced corrosion resistance while offered antibacterial properties and enhanced osteogenic activity in rat bone marrow mesenchymal stem cells [172]. Controlled Zn doping is vital to obtain these multifunctional properties, making the Mg implants toward multifunctional clinical application. Hiromoto et al. studied the comparison between carbonate apatite (CAp) and pure HAp coatings on Mg-0.8 mass% Ca (MgCa) alloys implanted in rabbit femurs, for both 8 and 24 weeks [173]. Both coatings initially prevented rapid corrosion, but CAp-coated devices underwent significantly less degradation as time progressed. Specifically, the CAp-coated implants showed no obvious corrosion pits and had a corrosion rate at 24 weeks half that of the HAp-coated implants and one-fifth that of the uncoated implants. The dissolution of the CAp coating gradually took place without causing any harm, especially in conjunction with areas of new bone attachment. This study highlights the great potential of CAp as a bioabsorbable layer for corrosion control and bone regeneration in orthopedic implants.

The hybrid coatings on the Mg alloys combine HAp, polymers, and oxides can offer improved corrosion resistance, bioactivity, and mechanical stability. Such multifunctional layers can develop into an interface for the bone, provide drug delivery, and protect the implants from rapid biodegrada-

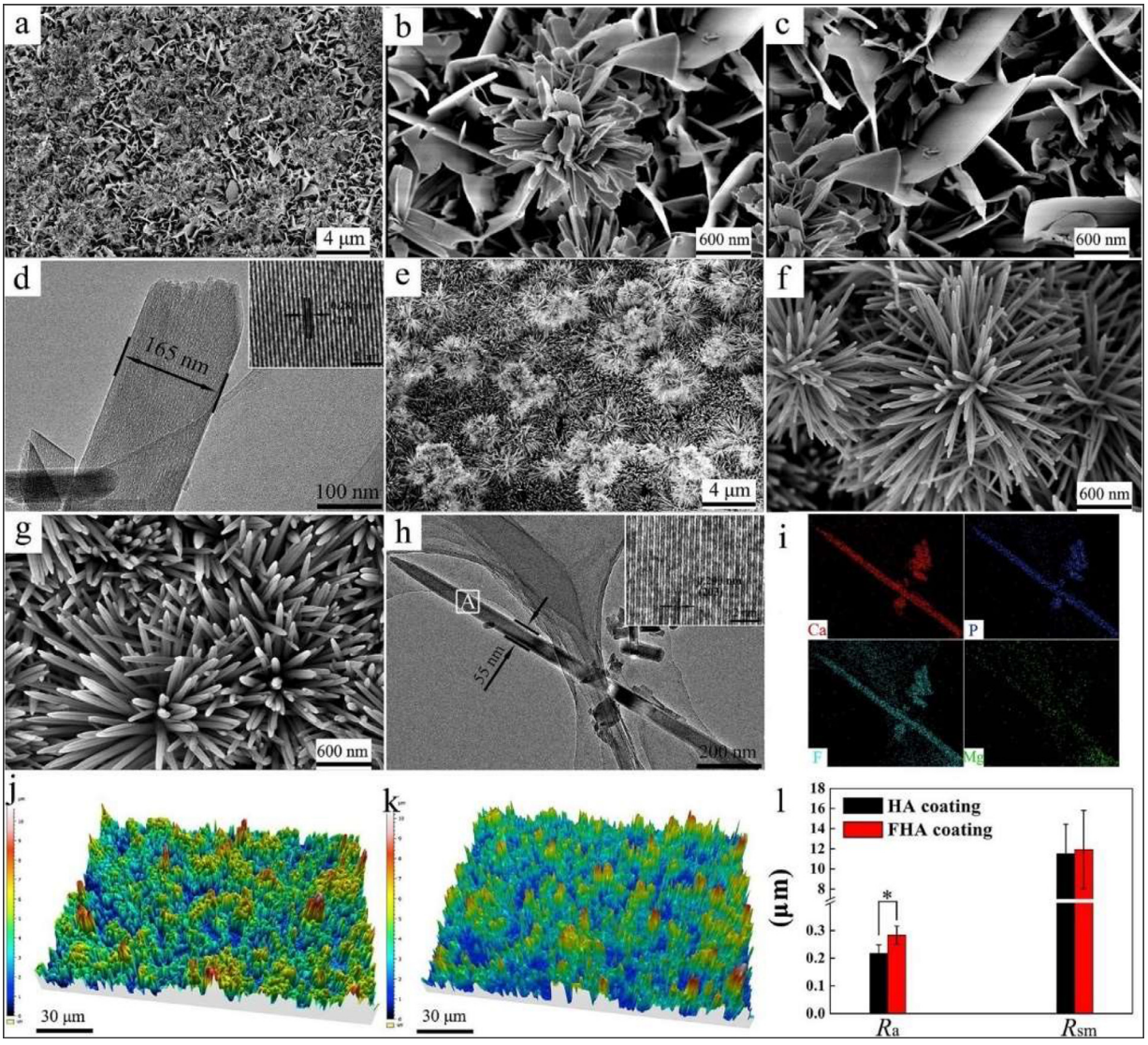

Fig. 19. Surface morphology and composition of the HAp and FHAp coatings. SEM and TEM images reveal nanosheets-like HAp coating (a–d), while a nanoneedles-like structure in FHAp coating (e–h). EDS mapping confirmed the elemental distribution (i). 3D profiling (j–k) and roughness analysis (l) demonstrated a higher degree of surface roughness and different topography for the FHAp coating (Reproduced with permission from Ref. [167]. License no: 6050090016926).

tion. Sreekanth et al. fabricated hybrid MgO/HAp composite coatings on an AZ31 Mg alloy via a PEO and EPD route [174]. The resultant coating exhibited good corrosion resistance against acidic (pH 4.5) and physiological (pH 7.4) environments. Structural analyses revealed HAp embedded within the MgO matrix in the coating, promoting surface passivation and osteoconductivity. Chen et al. produced carbonated HAp-graphene oxide composite coatings on AZ91 Mg alloy by ultrasonic-assisted electrophoretic deposition [175]. Ultrasonication simultaneously exfoliated graphene oxide nanosheets and aided CO_2 adsorption to induce in situ formation of B-type carbonated HAp. The carbonated HAp, graphene oxide, and graphene oxide-Mg complexes greatly improved corrosion resistance in saline environments, while the HAp-graphene oxide coating offers the best protective performance owing to denser microstructure and barrier effect. Askarnia et al. created a new composite coating composed of HAp, chitosan, and graphene oxide on AZ91D Mg alloy by the electrophoretic deposition method [176]. This work examined how varying graphene oxide content (0–2 wt%) impacted the coating's characteristics. The increase in graphene oxide content improved mechanical properties such as hardness (40–60 MPa) and Young's modulus (3.1–8 GPa). HAp precipitation and bioactivity were enhanced with higher graphene oxide content throughout 24 days of immersion in SBF. The corrosion resistance improvement is slightly noticeable, with corrosion rates decreasing from 4.3 to 0.2 mpy due to reduced surface cracking caused by the graphene oxide reinforcing effect. With 2 wt% graphene oxide in the composite coating, besides corrosion protection, strong antibacterial activity was found that could completely inhibit the growth of *Escherichia coli* and *S. aureus* after 24 h. These findings indicate the po-

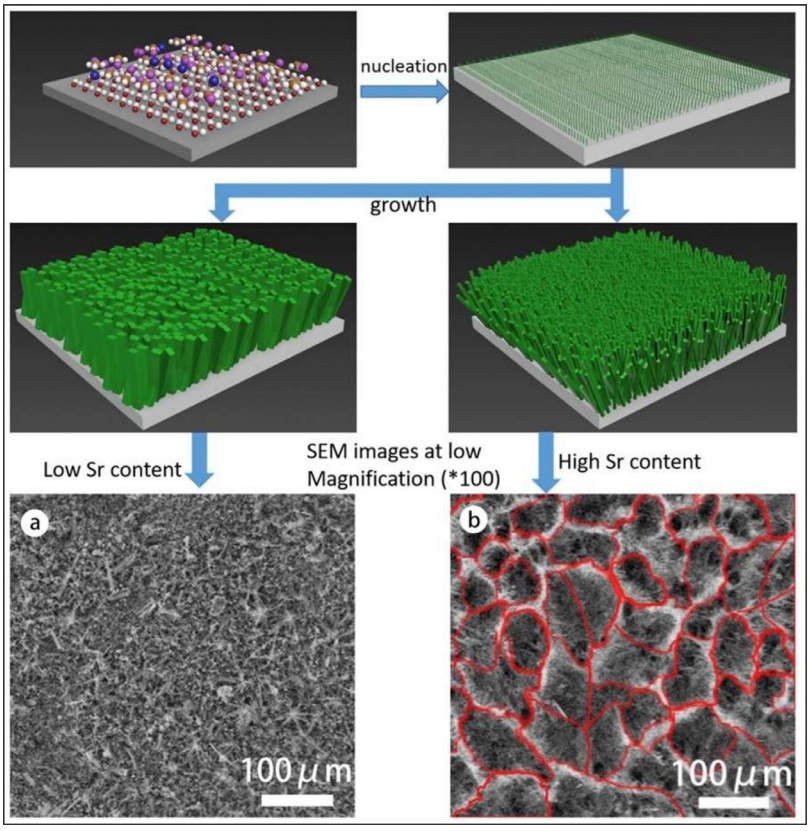

Fig. 20. Growth mechanism and SEM images of Sr 3% (a) and Sr 10% (b) HAp coatings on ZK60 Mg alloy (Reproduced with permission from Ref. [170]. License no: 6050170004220).

tential use of the coating for biodegradable orthopedic implant applications. Further, Zhang et al. fabricated composite coatings of polycaprolactone/HAp over AZ31 Mg alloy incorporating nanorod HAp crystals in the polycaprolactone polymer fill to improve adhesion and reduce corrosion rates by an order of magnitude as compared to a composite coating with HAp only [177]. This hybrid coating moderately supported BMSC cells' adhesion and cytocompatibility, although its antibacterial studies with methicillin-resistant *Staphylococcus aureus* demand further enhancement. Another hybrid system was reported by Tian et al., where they prepared a HAp/hydroxypropyltrimethyl ammonium chloride chitosan composite coating on Mg alloy having superhydrophilicity (~4° contact angle) to resist protein adsorption and bacterial adherence. The coating is highly antibacterial and kills about 99% of bacteria on *Staphylococcus aureus* and *Escherichia coli*, along with improved corrosion resistance and cytocompatibility. This study offer a suitable solution for combating implant-associated infections while ensuring biocompatibility [178]. Similarly, Ling et al. prepared copper-doped zeolitic imidazolate framework-8/HAp (Cu@ZIF-8/HAp) composite coatings onto AZ31B Mg alloy [179]. The dodecahedral Cu@ZIF-8 layer could function as a reservoir for controlled release of Cu^{2+} and Zn^{2+} ions for bacteria killing against *S. aureus* and *E. coli*, while the inner HAp layer can enhance cell adhesion and osteogenic activity. This multifunctional MOF-based coating demonstrates the synergistic effect of antimicrobial ion release with improved corrosion resistance and bioactivity (Fig. 22).

Stimuli-responsive coatings are a forefront topic in surface engineering for implants. Dynamic protection is achieved by changing their surface properties against environmental changes (such as pH or temperature) at the implant site. Zhang et al. reported crack-less HAp/phytic acid hybrid coatings formed by chemical conversion and hydrothermal treatment in saturated CaO solution [180]. While providing this effect, calcium and phosphate ions would first form amorphous CaP, which crystallized to HAp, repaired coating defects, and established excellent bonding strength with the substrate, as shown in Fig. 23. Meng et al. prepared a superhydrophobic HAp/Bi_2S_3/lauric acid composite coating with near-infrared (NIR) light-triggered wettability transition [181]. This smart coating could switch from hydrophobic to hydrophilic, thereby promoting cell adhesion when required, after NIR exposure and while resisting corrosion and antibacterial effectiveness (~99.9% against *S. aureus*). Further, an advanced multifunctional coating system was developed by Rahman et al., whereby they fabricated a 3-layered system from anodized oxide, HAp (via electrodeposition), and finally a hydrophobic silk fibroin top coat on Mg and WE43 alloys [182]. This coating reduced the corrosion rate by 50-fold in pure Mg and 26-fold in WE43. Additionally, the layers supported cell proliferation and reduced hydrogen evolution, where the anodized oxide induced microroughness, HAp pro-

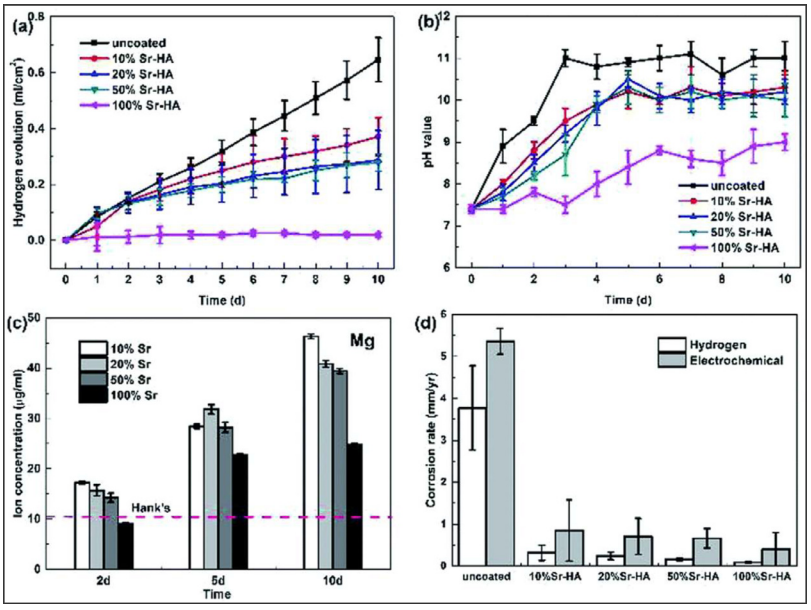

Fig. 21. (a) Hydrogen evolution, (b) pH change, (c) Mg release, and (d) corrosion rates of Sr-HA-coated Mg alloys in Hank's solution. Reproduced under Creative Commons license from Ref. [171].

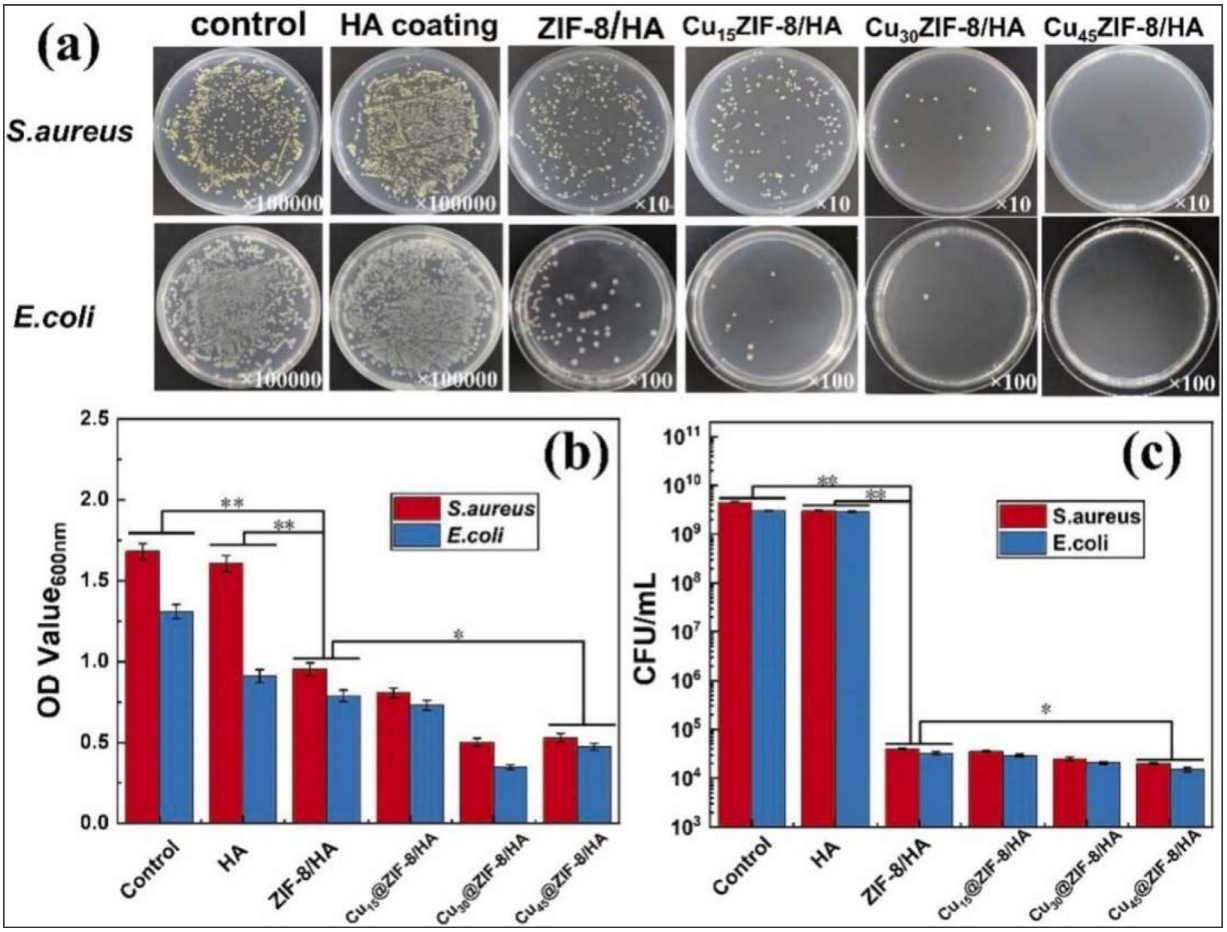

Fig. 22. (a) Photos of *S. aureus* and *E. coli* colonies after 24-h incubation at 37 °C with different coatings and blank control. (b) Bacterial viability and (c) colony count statistics on Cu@ZIF-8/HAp composite coatings after 24 h (Reproduced with permission from Ref. [179]. License no: 6050170877386).

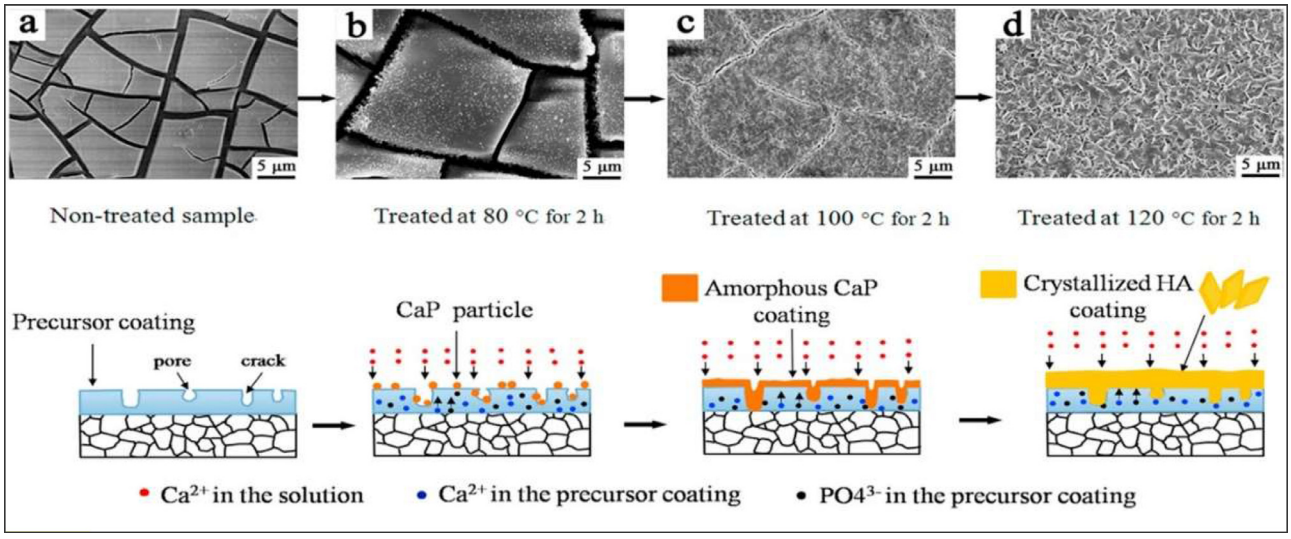

Fig. 23. SEM images with a schematic illustrating the HAp/phytic acid hybrid coating formation on AZ31 alloy. Defects in the untreated precursor (a) become less and less apparent after hydrothermal treatments at 80 °C (b), 100 °C (c), and 120 °C (d), where CaP is deposited and simultaneously CaP matures to crystallized HAp (Reproduced with permission from Ref. [180]. License no: 6050090299993).

vided mechanical hardness and bioactivity, and silk fibroin resisted water access and further corrosion. Zhai et al. studied ultrasonic spraying for coating silk fibroin /nHAp composites on microarc oxidized AZ31 Mg alloy [183]. The ultrasonic spraying allowed deep penetration into surface micropores, thus creating a mechanical interlocking and chemically stable bioactive layer. In vitro studies showed less hydrogen release and less degradation, while the in vivo implantation revealed low inflammatory responses and enhanced tissue regeneration. Researchers introduced the concept of tissue-reactive coatings, where early fibrous tissue interaction with the surface of an implant forms a protective barrier that regulates degradation and improves the integration of the substitute. Heakal et al. studied electrophoretic deposition of nanoHAp-ETELAC resin composite coatings on Mg-3Zn-0.8Ca alloy [184]. They synthesized nanoHAp by microwave-assisted hydrothermal synthesis and optimized deposition parameters to 50 V at 150 rpm, resulting in uniform, well-adherent, and crack-free coatings. Such protective coatings provided excellent corrosion resistance in SBF at 37 °C and reduced ion diffusion while at the same time maintaining mechanical integrity.

Drug-loaded HAp coatings bring new opportunities for multifunctionality, such that the coatings can also serve to deliver drugs locally and not simply act as a barrier against corrosion. The coating can be loaded with antibiotics, anti-inflammatory drugs, or growth factors to provide local, sustained release, thus fighting infections, promoting bone regeneration, and reducing systemic side effects. Ji et al. developed a gentamicin (GS)-loaded HAp coating on AZ31 Mg alloy by layer-by-layer assembly followed by hydrothermal treatment [185]. The schematic illustration (Fig. 24A) shows the layer-by-layer assembly of GS-loaded multilayers, followed by hydrothermal HAp growth. This process results in a denser and more compact coating, as shown by SEM (Fig. 24B). This structural improvement not only increases coating stability but also allows for effective antibacterial activity and a sustained release profile of GS, as demonstrated in the antibacterial assays and drug release studies (Fig. 24C). This GS-loaded HAp coating show enhanced corrosion resistance, antibacterial property, and excellent biocompatibility with gentamicin release up to 384 h. This study offer a prolonged protection against infection during the initial healing phase [185]. Similiarly, Gao et al. produced a calcium phosphate coating consisting of ciprofloxacin, with polyacrylic acid used as the templating agent during the hydrothermal synthesis [186]. The ciprofloxacin incorporated coating worked as an antimicrobial agent against both *S. aureus* and *E. coli*, while also supporting healthy cell growth with corrosion protection.

Rapid degradation of Mg implants impairs cytocompatibility and osseointegration, limiting their clinical application. To overcome this issue, Li et al. developed a bio-inspired bilayer coating, comprising an outer layer of HAp nanorods simulating osteoclastic bone nanotopography, and an inner pore-sealed layer of MgO prepared by microarc oxidation and hydrothermal treatment [187]. The coating acts by regulating intracellular ion concentrations and minimizing hydrogen evolution thus improving the mineralization of the extracellular matrix of osteoblasts. Meanwhile, the coating preferentially degrades at a controlled manner without causing delamination, thereby preserving its mechanical integrity and preventing osteolysis. This multifunctional coating represents a massive potential in the clinical translation of Mg-based implants by simultaneously addressing corrosion protection, osteoimmunomodulation, and osseo-integration. The huge advancements in nanostructuring, ion substitution, hybrid layering, and smart functionalities have allowed for tailored degradation rate, mechanical integrity, and biological response. Table 7 represents various HAp and HAp-based composite coatings applied on Mg alloys with different preparation methods

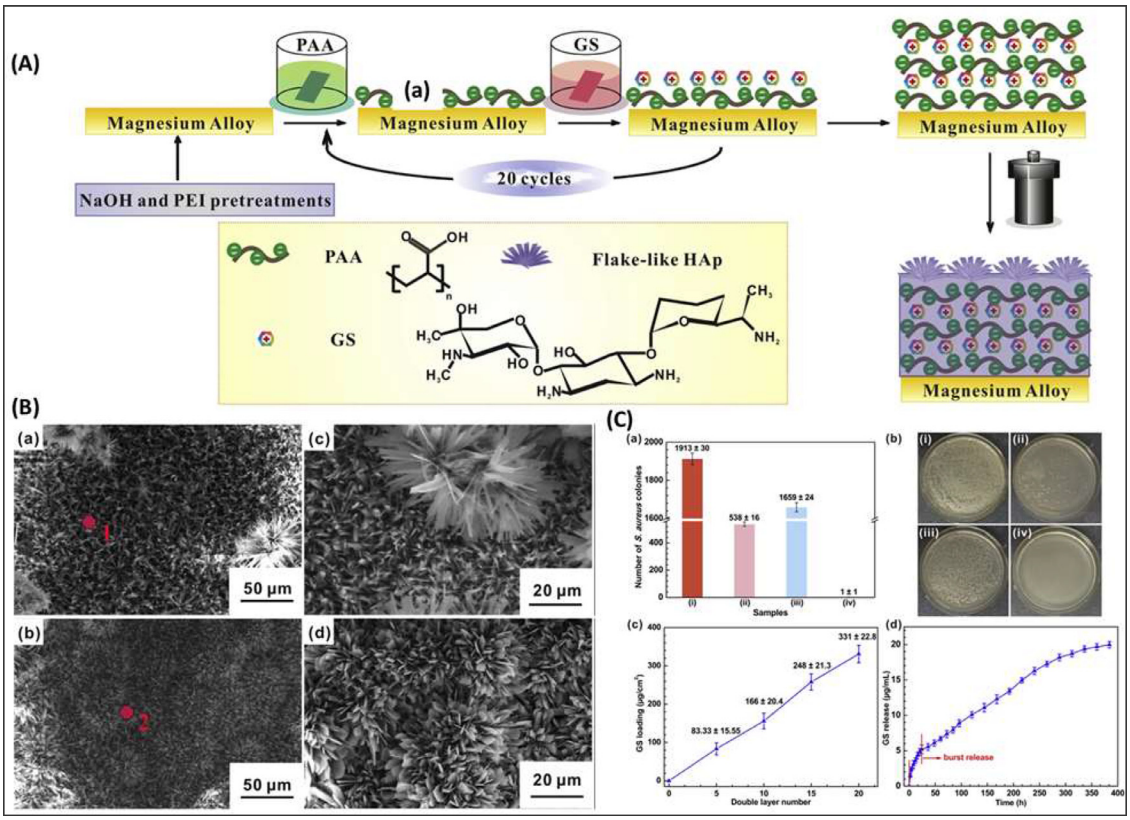

Fig. 24. (A) Schematic of GS-loaded HAp coating preparation. (B) SEM images of pure HAp (a, c) and GS-loaded HAp (b, d) coatings. (C) (a) *S. aureus* colony counts, (b) representative agar plates: (i) blank, (ii) AZ31, (iii) pure HAp, (iv) GS-loaded HAp, (c) GS loading with bilayer cycles, and (d) cumulative GS release profile in PBS medium (Reproduced with permission from Ref. [185]. License no: 6105160868873).

and electrolytes, thus comparing their efficacy in corrosion inhibition reported by several workers. This table clearly indicates that coating composition, preparation method, ion substitution, hybrid layering, and electrolyte condition greatly affect the corrosion behavior of Mg alloys. Composite coatings based on HAp and Sr-substituted HAp seem promising in increasing the life and safety of Mg-based implants for biomedical applications. These coatings can lower corrosion current density and shift corrosion potential to a positive side against degradation, thereby enhancing the biocompatibility and mechanical strength of Mg alloys. Serving as artificial bone minerals, these coatings also enhance drug delivery systems and antibacterial characteristics. Notable advancements of stimuli-responsive systems, dual-layer architectures, and the loading of therapeutic agents depict their capability of multiple functions. All of these developments favor HAp-coated Mg alloys as good candidates for next-generation bioresorbable orthopedic implantations with better clinical performance.

6. Challenges in HAp coatings on Mg alloys

Numerous scientific and technological challenges must be addressed to develop an effective and uniform HAp coating on Mg substrates [7,29,147]. One of the most significant challenges comes from how the Mg alloy is reactive to environmental factors during the deposition of coating layers. The highly electropositive character of Mg results in its rapid corrosion through oxidation and hydrogen evolution while in aqueous environments, particularly in coating methods that are aqueous-based such as electrochemical deposition or electrophoretic deposition [7,194–196]. The excessive reactivity inhibits good adhesion of the coating to the substrate, thus producing microcracks in the coating layer and causing non-uniform morphology due to gas evolution at the metal interface. Porosity is another drawback of HAp coatings, which allows penetration of body fluids and weakens the protective action, causing localized corrosion under the coating [7,8,196,197]. Another issue arises from the difficulty in obtaining strong interfacial bonds between HAp coatings and alloy substrate [5,29,194]. The mismatch in thermal expansion coefficients between the coating and alloys might introduce internal stresses [198]. Such stresses lead to delamination or cracking of the coating [192,193]. Additionally, Mg inherently tends to form a surface oxide layer that is loosely adherent and easily removable [7,121,174]. Surface pre-treatments such as acid etching, alkaline treatment, or anodization have been studied to improve surface roughness and coating adhesion, but optimizing these processes concerning different alloy compositions remains challenging [29,133,195].

Moreover, acheiving phase purity and crystallinity of the HAp coating is an important challenge [29,78]. The biological performance, cellular response, and host-tissue integra-

Table 7
Compares diverse HAp and HAp based coatings on Mg alloys produced through distinct methods and worked upon by various electrolyte solutions with different corrosion current densities and potentials.

Authors	Substrate	Coating sample	Preparation method	Electrolyte	I_{corr} (A/cm^2)	E_{corr} (V)	Corrosion rate (mm/yr)
Wang et al. [170]	ZK60 alloy	HAp	Hydrothermal	Hank's solution	5.09×10^{-6}	−1.39	1.16×10^{-4}
Wang et al. [170]	ZK60 alloy	Sr-HAp	Hydrothermal	Hank's solution	1.65×10^{-6}	−1.35	3.78×10^{-5}
Gu et al. [171]	AZ31B alloy	Sr-HAp	Electrodeposition	Hank's solution	17.55×10^{-6}	−1.47	0.5
Peng et al. [103]	AZ31 alloy	HAp/Mg(OH)$_2$	Hydrothermal	Hank's solution	4.879×10^{-8}	−1.355	0.92
Singh et al. [140]	AZ91 alloy	HAp-Bioglass	Electrophoretic deposition	SBF	542×10^{-6}	−1.486V	1.2
Singh et al. [140]	AZ91 alloy	HAp-Bioglass- chitosan-Fe_3O_4 composite	Electrophoretic deposition	SBF	398×10^{-6}	−1.422	0.090
Singh et al. [95]	Mg-Ag-Zn-Ca alloy	PA-HAp-PCL composite	Sol-gel	SBF	2.1×10^{-9}	−0.46	3.8×10^{-4}
Liao et al. [105]	AZ31B alloy	HAp/tea polyphenol	Hydrothermal	SBF	7.645×10^{-6}	−0.774	0.349
Liao et al. [105]	AZ31B alloy	HAp	Hydrothermal	SBF	7.949×10^{-6}	−0.789	0.363
Akbarzadeh et al. [188]	AZ91 Mg alloy	HAp	Electrodeposition	SBF	0.62×10^{-6}	−1.300	0.62
Sun et al. [189]	AZ31 magnesium alloy	HAp	Ultrasonic aqueous synthesis	SBF	5.56×10^{-6}	−1.57	0.94
Dunne et al. [190]	EW62	HAp	Spray coating	PBS	18.317×10^{-6}	−1.401	0.413
Ahangari et al. [191]	AZ31 magnesium alloy	HAp-carboxymethyl cellulose composite	Cathodic electrophoretic deposition	SBF	3.067×10^{-6}	−1.172	0.0683
Ahangari et al. [191]	AZ31 magnesium alloy	HAp-graphene composite	Cathodic electrophoretic deposition	SBF	2.960×10^{-6}	−1.037	0.0659
Ahangari et al. [191]	AZ31 magnesium alloy	HAp-carboxymethyl cellulose-graphene composite	Cathodic electrophoretic deposition	SBF	0.846×10^{-6}	−0.780	0.0188

tion are mainly depending on phase purity, crystallinity, and morphology of the HAp layer. Poorly crystallized or amorphous HAp may be bioreabsorbed too fast or may not provide sufficient bioactivity, whereas high crystalline coatings may be too brittle and may crack under mechanical stresses. The hardest part is producing the right crystallinity without compromising the substrate when low-temperature coatings are used, such as biomimetic deposition or sol-gel synthesis [7,120,192,199]. Moreover, another challenges in coating implants is achieving coating homogeneity over complex geometries, which may lead to incomplete coating or variable thickness [33,159,163,200]. Composite or multilayer coatings have therefore been examined as potential solutions. However, complexity in fabrication as well as concerns about biocompatibility and mechanical mismatch [105,106,195,201]. Laboratory-scale techniques may not be easily and directly brought into industrial-scale manufacturing while keeping the coating quality, especially for patient-specific or irregular-shaped implants [122,124,132,192]. The long-term behavior of HAp-coated Mg implants, in vivo biodegradation, and related processes remain with many existing research studies focusing mainly on short-term in vitro or small-animal models [122,192]. Finally, balancing bioactivity with degradation control has long been problematic [171,172,202]. Although HAp coatings promote biointegration with cell adhesion, proliferation, differentation, and mineralization, it may prevent the biodegradation of Mg implants that are intended to act as a temporary support [130,202]. To conclude, despite HAp coatings having significant potential for enhancing the performance of biodegradable Mg alloys with biomedical applications, currently few challenges including coating adhesion, long-term stability, biological response, and scalability should be addressed for specific applications.

7. Future trends and research directions

7.1. Multifunctional coatings

HAp coatings of the new generation in Mg alloys are expected to offer biocompatibility and corrosion resistance, have multimodal functions, and carry therapeutic agents to control infections during postoperative stages [22,203,204]. The growth factors can work as osteoinductive agents for increased bone regeneration [22,205]. The function of such composite coatings is to form a bioactive interface for the structure of the implant that helps in the healing process [206]. Also, developing it as a drug delivery system, where local therapy can be provided with reduced systemic side effects, thus enhancing patient outcomes [7,203]. These multifunctional coatings offer next generation implants in orthopedics and regenerative medicine [201,204,207].

7.2. Hybrid techniques

Hybrid coating techniques are used to optimize the performance of HAp coatings, which allow a synergy of deposition methods [75,184]. For instance, a biomimetic approach may

be integrated with electrochemical deposition or sol-gel methods to enhance both the biological affinity and mechanical stability of the coating [200,208]. Developing a multilayered or gradient structure by hybrid processes may exhibits a strong inner layer to offer good bonding to the Mg substrate and an outer layer that can be modified for enhanced bioactivity or drug delivery [195,209,210]. Hybridization also provides the capacity for imparting new nanoscale features or surface textures that can promote osteoblast adhesion and proliferation with antibacterial activity [104,207,211]. Incorporating two different approaches creates a very flexible and customizable platform to engineer coatings for specific clinical applications.

7.3. Smart coatings

The evolution of smart coatings represents an innovative approach in implant technology [179,185,212]. These smart surfaces are designed to respond dynamically to changes in the physiological environment, such as pH, temperature, or biochemical signals. For instance, a smart HAp coating may remain inert under normal conditions but release anti-inflammatory or antimicrobial agents in response to infection or inflammation [213–215]. Other coatings may degrade at a rate influenced by the surrounding pH, aligning more precisely with tissue regeneration. Recent research has also explored the use of shape-memory polymers, piezoelectric materials, and stimuli-responsive hydrogels integrated with HAp to create coatings capable of self-healing, releasing drugs on-demand, or even altering their mechanical properties in situ [152,213,215–217]. These innovations aim to reduce the risk of implant failure and promote a more adaptive healing process. This may offer a new paradigm of self-regulating biomedical devices [214,218].

7.4. 3D-printed scaffolds

Integrating HAp coating with a 3D-printed Mg scaffold is an excellent approach for patient-specific treatments [214,218,219]. Additive manufacturing can impart highly custom geometries to implants that mirror patient-specific anatomical features, mainly for complicated orthopedic or maxillofacial reconstructions [218,220]. The HAp coating ensures these scaffolds act as promising scaffolds for supporting structural integrity and promoting fast bone in-growth and remodeling. Secondly, the 3D-printed scaffolds allow accurate design control over matrix porosity and interconnectivity, and these parameters are critical for nutrients to pass through, vascularization, and host tissue integration [219,221,222]. With continued advancement in digital design tools and bioprinting technologies, the combination of HAp-coated 3D printed Mg scaffolds can be used for patient-specific implant therapy [218,221,223].

8. Conclusion

Mg alloys are an excellent candidate for temporary medical implants, especially from an orthopedic and dental applications, owing to their biodegradability, biocompatibility, and mechanical properties similar to bones. However, the fast corrosion of Mg alloys in physiological environments should be considered a primary concern. Hence, HAp coatings are considered a practical solution to this problem as they improve corrosion resistance while enhancing osteoconductivity and bioactivity. In this review, we have summarized the latest developments in various HAp coating techniques on Mg alloy. While much progress has been made toward corrosion resistance, biocompatibility, and biological performance of HAp-coated Mg alloys, further research is required on hybrid coating techniques and functionalization strategies to enhance long-term coating stability, controllable degradation rates, and reproducibility at a large scale. Long-term clinical studies on HAp-based hybrid and composite coatings are needed to bring Mg-based alloys for next-generation implant materials.

Declaration of generative AI and AI-assisted technologies in the writing process

During the preparation of this work, the authors used Grammarly with caution to improve language and readability. After using this tool, the authors reviewed and edited the content as needed and take full responsibility for the content of the publication.

Declaration of competing interest

The authors declare that they have no known competing financial interests or personal relationships that could have appeared to influence the work reported in this paper.

CRediT authorship contribution statement

G. Suresh Kumar: Writing – original draft, Investigation, Conceptualization. **K. Lalithambigai:** Visualization, Formal analysis, Data curation. **Nguyen Van Minh:** Writing – review & editing, Software, Resources, Formal analysis. **Mohd. Shkir:** Writing – review & editing, Validation, Resources, Funding acquisition. **M.A. Sayed:** Writing – review & editing, Visualization, Software, Formal analysis.

Acknowledgment

The authors extend their appreciation to the Deanship of Research and Graduate Studies at King Khalid University for funding this work through Small Group Research Project under grant number RGP1/34/46 (RGP1/34/46).

References

[1] S. Agarwal, J. Curtin, B. Duffy, S. Jaiswal, Mater. Sci. Eng. C 68 (2016) 948–963, doi:10.1016/J.MSEC.2016.06.020.
[2] N. Sezer, Z. Evis, S.M. Kayhan, A. Tahmasebifar, M. Koç, J. Magnes. Alloy 6 (2018) 23–43, doi:10.1016/j.jma.2018.02.003.
[3] M. Ali, M.A. Hussein, N. Al-Aqeeli, J. Alloys Compd. 792 (2019) 1162–1190, doi:10.1016/J.JALLCOM.2019.04.080.
[4] J. Singh, A.Wahab Hashmi, S. Ahmad, Y. Tian, Inorg. Chem. Commun. 169 (2024) 113111, doi:10.1016/j.inoche.2024.113111.

[5] M.C.L. de Oliveira, R.M.P. da Silva, R.M. Souto, R.A. Antunes, J. Magnes. Alloys 12 (2024) 3062–3093, doi:10.1016/J.JMA.2024.07.030.
[6] F.Z. Akbarzadeh, M. Sarraf, E.R. Ghomi, V.V. Kumar, M. Salehi, S. Ramakrishna, S. Bae, J. Magnes. Alloys 12 (2024) 2569–2594, doi:10.1016/J.JMA.2024.06.015.
[7] M. Rahman, Y. Li, C. Wen, J. Magnes, Alloys 8 (2020) 929–943, doi:10.1016/j.jma.2020.05.003.
[8] J. Yang, Z. Zhang, W. Yao, Y. Wu, Y. Gao, Y. Yang, L. Wu, M. Serdechnova, C. Blawert, F. Pan, J. Magnes. Alloys 13 (2025) 1405–1427, doi:10.1016/J.JMA.2025.01.027.
[9] M. Niinomi, Metall. Mater. Trans. A 33 (2002) 477–486, doi:10.1007/s11661-002-0109-2.
[10] P. Balakrishnan, M.S. Sreekala, S. Thomas, Fundamental Biomaterials: Metals, Woodhead Publishing, Sawston, Cambridge, 2018, doi:10.1016/C2016-0-03502-7.
[11] M. Niinomi, M. Nakai, J. Hieda, Acta Biomater. 8 (2012) 3888–3903, doi:10.1016/j.actbio.2012.06.037.
[12] T. Odaira, S. Xu, K. Hirata, X. Xu, T. Omori, K. Ueki, K. Ueda, T. Narushima, M. Nagasako, S. Harjo, T. Kawasaki, L. Bodnárová, P. Sedlák, H. Seiner, R. Kainuma, Adv. Mater. 34 (2022) 2202305, doi:10.1002/adma.202202305.
[13] X. Yan, W. Cao, H. Li, Materials 15 (2022) 66, doi:10.3390/ma15010066.
[14] S. Xiaoxiu, M. Shilong, L. Yang, M. Xingshuang and L. Yanfeng, 25 (2021) 593–599, doi:10.3969/j.issn.2095-4344.2374.
[15] A. Bordbar-Khiabani, B. Yarmand, M. Mozafari, Emerg. Mater. 8 (3) (2019) 305–319.
[16] K.K. Thomas, M.N. Zafar, W.G. Pitt, G.A. Husseini, Appl. Sci. 14 (2023) 10, doi:10.3390/app14010010.
[17] A.M. Al Alawi, S.W. Majoni, H. Falhammar, Int. J. Endocrinol. 2018 (2018) 1–17, doi:10.1155/2018/9041694.
[18] Y. Chen, Z. Xu, C. Smith, J. Sankar, Acta Biomater. 10 (2014) 4561–4573, doi:10.1016/j.actbio.2014.07.005.
[19] M.P. Staiger, A.M. Pietak, J. Huadmai, G. Dias, Biomaterials 27 (2006) 1728–1734, doi:10.1016/j.biomaterials.2005.10.003.
[20] K. Glenske, P. Donkiewicz, A. Köwitsch, N. Milosevic-Oljaca, P. Rider, S. Rofall, J. Franke, O. Jung, R. Smeets, R. Schnettler, S. Wenisch, M. Barbeck, Int. J. Mol. Sci. 19 (2018) 826, doi:10.3390/IJMS19030826.
[21] X. Liang, T. Tong, C. Xian, J. Du, B. Tan, L. Wang, J. Hou, J. Wu, Chin. Chem. Lett. (2025) 111140, doi:10.1016/J.CCLET.2025.111140.
[22] D. Bairagi, S. Mandal, J. Magnes. Alloys 10 (2022) 627–669, doi:10.1016/j.jma.2021.09.005.
[23] M. Nasr Azadani, A. Zahedi, O.K. Bowoto, B.I. Oladapo, Prog. Biomater. 11 (1) (2022) 1–26, doi:10.1007/S40204-022-00182-X.
[24] S. Kamrani, C. Fleck, BioMetals 32 (2019) 185–193, doi:10.1007/S10534-019-00170-Y.
[25] N. Wang, S. Yang, H. Shi, Y. Song, H. Sun, Q. Wang, L. Tan, S. Guo, J. Magnes, Alloys 10 (2022) 3327–3353, doi:10.1016/j.jma.2022.11.014.
[26] U. Riaz, I. Shabib, W. Haider, J. Biomed. Mater. Res. B Appl. Biomater. 107 (2019) 1970–1996, doi:10.1002/JBM.B.34290.
[27] J. Chen, L. Tan, X. Yu, I.P. Etim, M. Ibrahim, K. Yang, J. Mech. Behav. Biomed. Mater. 87 (2018) 68–79, doi:10.1016/J.JMBBM.2018.07.022.
[28] J.-W. Lee, H.-S. Han, K.-J. Han, J. Park, H. Jeon, M.-R. Ok, H.-K. Seok, J.-P. Ahn, K.E. Lee, D.-H. Lee, S.-J. Yang, S.-Y. Cho, P.-R. Cha, H. Kwon, T.-H. Nam, J.H. Lo Han, H.-J. Rho, K.-S. Lee, Y.-C. Kim, D. Mantovani 113 (2016) 716–721, doi:10.1073/pnas.1518238113.
[29] A.M. Zhang, P. Lenin, R.C. Zeng, M.B. Kannan, J. Magnes. Alloys 10 (2022) 1154–1170, doi:10.1016/J.JMA.2022.01.001.
[30] J. Kuhlmann, I. Bartsch, E. Willbold, S. Schuchardt, O. Holz, N. Hort, D. Höche, W.R. Heineman, F. Witte, Acta Biomater. 9 (2013) 8714–8721, doi:10.1016/j.actbio.2012.10.008.
[31] J. Gonzalez, R.Q. Hou, E.P.S. Nidadavolu, R. Willumeit-Römer, F. Feyerabend, Bioact. Mater. 3 (2018) 174–185, doi:10.1016/j.bioactmat.2018.01.003.
[32] J. Yang, F. Cui, I.Seop. Lee, Ann. Biomed. Eng. 39 (2011) 1857–1871, doi:10.1007/s10439-011-0300-y.
[33] P. Tong, Y. Sheng, R. Hou, M. Iqbal, L. Chen, J. Li, Smart. Mater. Med. 3 (2022) 104–116, doi:10.1016/j.smaim.2021.12.007.
[34] S. Amukarimi, M. Mozafari, MedComm (Beijing) 2 (2021) 123–144, doi:10.1002/mco2.59.
[35] S.M. Kim, J.H. Jo, S.M. Lee, M.H. Kang, H.E. Kim, Y. Estrin, J.H. Lee, J.W. Lee, Y.H. Koh, J. Biomed. Mater. Res. A 102 (2014) 429–441, doi:10.1002/JBM.A.34718.
[36] S.V. Dorozhkin, Materials 2 (2009) 399–498, doi:10.3390/ma2020399.
[37] M. Vallet-Regí, J.M. González-Calbet, Prog. Solid State Chem. 32 (2004) 1–31, doi:10.1016/j.progsolidstchem.2004.07.001.
[38] J.C. Elliott, Structure and Chemistry of the Apatites and Other Calcium Orthophosphates, Elsevier, Amsterdam, Netherlands, 1994.
[39] M. Mucalo, Hydroxyapatite (HAp) for Biomedical Applications, Woodhead Publishing, Sawston, Cambridge, 2015, doi:10.1016/C2013-0-16440-9.
[40] Y. Hong, H. Fan, B. Li, B. Guo, M. Liu, X. Zhang, Mater. Sci. Eng. R Rep. (2010) 225–242, doi:10.1016/j.mser.2010.06.010.
[41] S.V. Dorozhkin, Am. J. Biomed. Eng. 2 (2012) 48–97, doi:10.5923/j.ajbe.20120203.01.
[42] M. Vallet-Regí, D.A. Arcos, RSC Publishing, Cambridge, England, 2008,.
[43] W.R. Wagner, S.E. Sakiyama-Elbert, G. Zhang, M.J. Yaszemski, Biomaterials science: An introduction to materials in medicine, Academic Press, an imprint of Elsevier, London, 2020, doi:10.1016/C2017-0-02323-6.
[44] E. Boanini, M. Gazzano, A. Bigi, Acta Biomater. 6 (2010) 1882–1894, doi:10.1016/j.actbio.2009.12.041.
[45] T. Sakae, H. Nakada, J.P. LeGeros, J. Hard Tissue. Biol. 24 (2015) 111–122, doi:10.2485/jhtb.24.111.
[46] A. Haider, S. Haider, S.S. Han, I.K. Kang, RSC Adv. 7 (2017) 7442–7458, doi:10.1039/c6ra26124h.
[47] C. Gao, S. Peng, P. Feng, C. Shuai, Bone Res. 5 (2017) 17059, doi:10.1038/boneres.2017.59.
[48] S.V. Dorozhkin, Acta Biomater. 6 (2010) 715–734, doi:10.1016/j.actbio.2009.10.031.
[49] M.I. Kay, R.A. Young, A.S. Posner, Nature 204 (1964) 1050–1052, doi:10.1038/2041050a0.
[50] A.S. Posner, A. Perloff, A.F. Diorio, Acta Crystallogr. 11 (1958) 308–309, doi:10.1107/s0365110x58000815.
[51] A. Ressler, A. Žužić, I. Ivanišević, N. Kamboj, H. Ivanković, Open Ceramics 6 (2021) 100122, doi:10.1016/J.OCERAM.2021.100122.
[52] K. Momma, F. Izumi, J. Appl. Crystallogr. 44 (2011) 1272–1276, doi:10.1107/S0021889811038970.
[53] J. Lu, H. Yu, C. Chen, RSC Adv. 8 (2018) 2015–2033, doi:10.1039/c7ra11278e.
[54] X. Hou, L. Zhang, Z. Zhou, X. Luo, T. Wang, X. Zhao, B. Lu, F. Chen, L. Zheng, J. Funct. Biomater. 13 (2) (2022) 187, doi:10.3390/jfb13040187.
[55] G.S. Kumar, E.K. Girija, A. Thamizhavel, Y. Yokogawa, S.N. Kalkura, J. Colloid Interface Sci. 349 (2010) 56–62, doi:10.1016/j.jcis.2010.05.038.
[56] S.J. Kalita, A. Bhardwaj, H.A. Bhatt, Mater. Sci. Eng. C 27 (2007) 441–449, doi:10.1016/j.msec.2006.05.018.
[57] H. Zhou, J. Lee, Acta Biomater. 7 (2011) 2769–2781, doi:10.1016/j.actbio.2011.03.019.
[58] S. Pokhrel, Adv. Chem. Eng. Sci. 8 (2018) 225–240, doi:10.4236/aces.2018.84016.
[59] M. Ramalingam, X. Wang, G. Chen, P.X. Ma, F.-Z. Cui, Biomimetics: Advancing nanobiomaterials and Tissue Engineering, John Wiley & Sons, Hoboken, NJ, 2013.
[60] S. Wu, X. Liu, C. Gao, Sci. Bull. 60 (2015) 691–700, doi:10.1007/s11434-015-0753-8.
[61] C. Liu, M. Xu, Y. Wang, Q. Yin, J. Hu, H. Chen, Z. Sun, C. Liu, X. Li, W. Zhou, H. Liu, Mater. Sci. Eng. R Rep. 161 (2024) 100870, doi:10.1016/j.mser.2024.100870.

[62] J. Jeong, J.H. Kim, J.H. Shim, N.S. Hwang, C.Y. Heo, Biomater. Res. 23 (2019) 4, doi:10.1186/s40824-018-0149-3.
[63] S. Lara-Ochoa, W. Ortega-Lara, C.E. Guerrero-Beltrán, Pharmaceutics 13 (2021) 1642, doi:10.3390/pharmaceutics13101642.
[64] M. Sundar Raj, V.H. Arkin, M.Jagannath Adalarasu, Indian J. Sci. Technol. 6 (2013) 1–6, doi:10.17485/ijst/2013/v6isp5.18.
[65] P. Agalya, S. Cholan, K.M. Prabu, G.S. Kumar, G. Karunakaran, M. Shkir, E. Kolesnikov, S. Ramalingam, Inorg. Chem. Commun. 143 (2022) 109788, doi:10.1016/j.inoche.2022.109788.
[66] K. Lin, J. Pan, Y. Chen, R. Cheng, X. Xu, J. Hazard. Mater. 161 (2009) 231–240, doi:10.1016/j.jhazmat.2008.03.076.
[67] Y. Zhang, Y.J. Zhu, H.P. Yu, Molecules 27 (15) (2022) 5020, doi:10.3390/molecules27155020.
[68] M. Kasprzak, A. Szabłowska, A. Kurzyk, P. Tymowicz-Grzyb, A. Najmrodzki, A. Woźniak, A. Antosik, J. Pagacz, P. Szterner, A. Plichta, P. Wieciński, P. Rusek-Wala, A. Krupa, P. Płociński, K. Rudnicka, M. Biernat, Int. J. Mol. Sci. 23 (18) (2022) 10454, doi:10.3390/ijms231810454.
[69] Y. Wang, W. Xu, Y. Lu, W. Xu, H. Yin, G. Xiao, Mater. Sci. Eng. C 108 (2020) 110408, doi:10.1016/j.msec.2019.110408.
[70] Y. Jia, L. Qin, Y. Gong, R. Chen, Y. Yang, W. Yang, K. Cai, J. Biomed. Mater. Res. A 109 (5) (2021) 804–813, doi:10.1002/jbm.a.37068.
[71] J. Xiao, Y. Zhu, Q. Ruan, Y. Liu, Y. Zeng, F. Xu, L. Zhang, Cryst. Growth Des. 10 (2010) 1492–1499, doi:10.1021/cg9001016.
[72] B. Ma, J. Han, S. Zhang, F. Liu, S. Wang, J. Duan, Y. Sang, H. Jiang, D. Li, S. Ge, J. Yu, H. Liu, Acta Biomater. 71 (2018) 108–117, doi:10.1016/J.ACTBIO.2018.02.033.
[73] F. Chen, Y.-J. Zhu, X.-Y. Zhao, B.-Q. Lu, J. Wu, CrystEngComm 15 (2013) 4527, doi:10.1039/c3ce40115d.
[74] Y. Liu, Y. Tang, J. Wu, J. Sun, X. Liao, Z. Teng, G. Lu, J. Colloid Interface Sci. 570 (2020) 402–410, doi:10.1016/j.jcis.2020.03.010.
[75] X. Zhao, Y. Zhu, C. Qi, F. Chen, B. Lu, J. Zhao, J. Wu, Chem. Asian J. 8 (2013) 1313–1320, doi:10.1002/asia.201300142.
[76] Y. Wang, M.S. Hassan, P. Gunawan, R. Lau, X. Wang, R. Xu, J. Colloid Interface Sci. 339 (2009) 69–77, doi:10.1016/j.jcis.2009.07.023.
[77] Y. Zhang, Y. Liu, X. Ji, C.E. Banks, W. Zhang, Chem. Commun. 47 (2011) 4126–4128, doi:10.1039/c1cc10489f.
[78] B. Beig, U. Liaqat, M.F.K. Niazi, I. Douna, M. Zahoor, M.B.K. Niazi, Coatings 10 (12) (2020) 1249, doi:10.3390/coatings10121249.
[79] K. Rezwan, Q.Z. Chen, J.J. Blaker, A.R. Boccaccini, Biomaterials 27 (2006) 3413–3431, doi:10.1016/j.biomaterials.2006.01.039.
[80] M. Aminzare, A. Eskandari, M.H. Baroonian, A. Berenov, Z. Razavi Hesabi, M. Taheri, S.K. Sadrnezhaad, Ceram. Int. 39 (2013) 2197–2206, doi:10.1016/j.ceramint.2012.09.023.
[81] P. Agalya, T. Saravanan, G.S. Kumar, S. Cholan, G. Karunakaran, N. Van Minh, Optik 225 (2021) 165564, doi:10.1016/j.ijleo.2020.165564.
[82] T. Zhang, W. Wang, J. Liu, L. Wang, Y. Tang, K. Wang, Front. Bioeng. Biotechnol. 10 (2022) 953344, doi:10.3389/fbioe.2022.953344.
[83] V. Tsakiris, C. Tardei, F.M. Clicinschi, J. Magnes. Alloys, 9 (2022) 1884–1905, doi:10.1016/j.jma.2021.06.024.
[84] S.V. Dorozhkin, Acta Biomater. 10 (2014) 2919–2934, doi:10.1016/j.actbio.2014.02.026.
[85] T.S.N. Sankara Narayanan, I.-S. Park, M.H. Lee, Surface modification of magnesium and its alloys for biomedical applications, modification and Coating Techniques, 2, Woodhead Publishing, Cambridge, UK, 2015, doi:10.1016/C2013-0-16448-3.
[86] D. Wang, G.P. Bierwagen, Prog. Org. Coat. 64 (2009) 327–338, doi:10.1016/j.porgcoat.2008.08.010.
[87] A. Jaafar, C. Hecker, P. Árki, Y. Joseph, Bioengineering 7 (4) (2020) 127, doi:10.3390/bioengineering7040127.
[88] J. Wright, N. Sommerdijk, Sol-gel materials: Chemistry and applications, CRC Press, Boca Raton, FL, 2014, doi:10.1201/9781315273808.
[89] R. Rojaee, M. Fathi, K. Raeissi, Mater. Sci. Eng. C 33 (2013) 3817–3825, doi:10.1016/j.msec.2013.05.014.
[90] E. Tranquillo, F. Bollino, Coatings 10 (6) (2020) 589, doi:10.3390/COATINGS10060589.
[91] S. Singh, R. Manoj Kumar, K.K. Kuntal, P. Gupta, S. Das, R. Jayaganthan, P. Roy, D. Lahiri, JOM. 67 (2015) 702–712, doi:10.1007/s11837-015-1364-1.
[92] X. Ye, S. Cai, G. Xu, Y. Dou, H. Hu, X. Ye, H. Zhao, X. Sun, J. Electrochem. Soc. 161 (2014) C145, doi:10.1149/2.091403jes.
[93] A. Sadeghi Larimi, H. Jafari, A. Sadeghzadeh, JOM. 76 (2024) 7186–7197, doi:10.1007/s11837-024-06932-5.
[94] A. Roy, S.S. Singh, M.K. Datta, B. Lee, J. Ohodnicki, P.N. Kumta, Mater. Sci. Eng. B 176 (2011) 1679–1689, doi:10.1016/j.mseb.2011.08.007.
[95] A. Singh, U. Batra, M. Sharma, J. Ind. Eng. Chem. 147 (2022) 293–303, doi:10.1016/j.jiec.2024.12.020.
[96] J. Gao, X.-D. Li, Y.-X. Gai, K. Wang, M. Li, J.-X. Dong, H.-Y. Cai, L.-Y. Cui, S.-Q. Li, Surf. Coat. Technol. 496 (2025) 131681, doi:10.1016/j.surfcoat.2024.131681.
[97] C. Jayakrishnan, S.R. Sheeja, G.S. Kumar, K. Lalithambigai, J. Duraimurugan, M.M. Alam, J. Solgel. Sci. Technol. 112 (2024) 262–276, doi:10.1007/s10971-024-06515-5.
[98] K. Byrappa, T. Adschiri, Prog. Cryst. Growth Charact. Mater. 53 (2007) 117–166, doi:10.1016/j.pcrysgrow.2007.04.001.
[99] Y.X. Gan, A.H. Jayatissa, Z. Yu, X. Chen, M. Li, J. Nanomater. (2020) 8917013, doi:10.1155/2020/8917013.
[100] S. Wen, X. Liu, J. Ding, Y. Liu, Z. Lan, Z. Zhang, G. Chen, Prog. Nat. Sci. Mater. Int. 31 (2021) 324–333, doi:10.1016/j.pnsc.2020.12.013.
[101] D. He, X. Zhang, P. Liu, X. Liu, X. Chen, F. Ma, W. Li, K. Zhang, H. Zhou, Surf. Coat. Technol. 406 (2022) 126656, doi:10.1016/j.surfcoat.2020.126656.
[102] D. Jiang, Y.-Z. Liu, B. Li, S. Chen, S.-Q. Li, W.-J. Yang, L.-Y. Cui, R.-C. Zeng, Appl. Surf. Sci. 614 (2023) 156041, doi:10.1016/j.apsusc.2022.156041.
[103] C. Peng, K. Qi, Y. Qiu, X. Guo, Surf. Interfaces 69 (2025) 106737, doi:10.1016/j.surfin.2025.106737.
[104] B. Zheng, H. Li, J. Wang, W. Wu, J. Ou, C. Shen, J. Mater. Res. 37 (2022) 1810–1824, doi:10.1557/s43578-022-00588-0.
[105] J. Liao, X. Li, G. Li, Surf. Coat. Technol. 511 (2025) 132282, doi:10.1016/j.surfcoat.2025.132282.
[106] H. Zhang, S. Cai, H. Zhang, L. Ling, Y. Zuo, H. Tian, T. Meng, G. Xu, X. Bao, M. Xue, Front. Mater. Sci. 18 (2024) 240678, doi:10.1007/s11706-024-0678-8.
[107] J. Liao, X. Li, S. Xuan, W. Zhang, G. Li, H. Li, Chem. Eng. J. 495 (2024) 153550, doi:10.1016/j.cej.2024.153550.
[108] Z. Zhou, B. Zheng, Y. Gu, C. Shen, J. Wen, Z. Meng, S. Chen, J. Ou, A. Qin, Surf. Interfaces 19 (2020) 100501, doi:10.1016/j.surfin.2020.100501.
[109] T. Kokubo, S. Yamaguchi, J. Biomed. Mater. Res. A 107 (2019) 968–977, doi:10.1002/jbm.a.36620.
[110] B. Yilmaz, A.E. Pazarceviren, A. Tezcaner, Z. Evis, Microchem. J. 155 (2020) 104713, doi:10.1016/j.microc.2020.104713.
[111] A. Oyane, H.M. Kim, T. Furuya, T. Kokubo, T. Miyazaki, T. Nakamura, J. Biomed. Mater. Res. A 65 (2003) 188–195, doi:10.1002/jbm.a.10482.
[112] A.C. Tas, Biomaterials 21 (2000) 1429–1438, doi:10.1016/S0142-9612(00)00019-3.
[113] A. Bigi, E. Boanini, B. Bracci, A. Facchini, S. Panzavolta, F. Segatti, L. Sturba, Biomaterials 26 (2005) 4085–4089, doi:10.1016/J.BIOMATERIALS.2004.10.034.
[114] P. Habibovic, F. Barrère, C.A. Van Blitterswijk, K. De Groot, P. Layrolle, J. Am. Ceram. Soc. 85 (2002) 517–522, doi:10.1111/j.1151-2916.2002.tb00126.x.
[115] T. Aviles, S.M. Hsu, A. Clark, F. Ren, C. Fares, P.H. Carey, J.F. Esquivel-Upshaw, Materials 13 (24) (2020) 5593, doi:10.3390/ma13245593.
[116] Y. Yang, Y. Wu, Y. Wei, T. Zeng, B. Cao, J. Liang, Materials 14 (2021) 1849, doi:10.3390/ma14081849.
[117] F. Gao, C. Xu, H. Hu, Q. Wang, Y. Gao, H. Chen, Q. Guo, D. Chen, D. Eder, Mater. Lett. 138 (2015) 25–28, doi:10.1016/j.matlet.2014.09.088.

[118] B. Zhu, Y. Xu, J. Sun, L. Yang, C. Guo, J. Liang, B. Cao, Metals 7 (2017) 214, doi:10.3390/met7060214.
[119] B. Lin, M. Zhong, C. Zheng, L. Cao, D. Wang, L. Wang, J. Liang, B. Cao, Surf. Coat. Technol. 281 (2015) 82–88, doi:10.1016/j.surfcoat.2015.09.033.
[120] W. Cui, E. Beniash, E. Gawalt, Z. Xu, C. Sfeir, Acta Biomater. 9 (2013) 8650–8659, doi:10.1016/j.actbio.2013.06.031.
[121] L. Hernández, J.E. González, V. Barranco, Y. Veranes-Pantoja, J.C. Galván, G.R. Gattorno, Ceram. Int. 48 (2022) 1208–1222, doi:10.1016/J.CERAMINT.2021.09.206.
[122] T.T. Li, L. Ling, M.C. Lin, H.K. Peng, H.T. Ren, C.W. Lou, J.H. Lin, J. Mater. Sci. 55 (2020) 6352–6374, doi:10.1007/s10853-020-04467-z.
[123] Y.W. Song, D.Y. Shan, E.H. Han, Mater. Lett. 62 (2008) 3276–3279, doi:10.1016/j.matlet.2008.02.048.
[124] C.M. Cotrut, A. Vladescu, M. Dinu, D.M. Vranceanu, Ceram. Int. 44 (2018) 669–677, doi:10.1016/j.ceramint.2017.09.227.
[125] P.R. Dev, C.P. Anand, D.S. Michael, P. Wilson, Mater. Adv. 3 (2022) 7773–7809, doi:10.1039/D2MA00620K.
[126] M. Jamesh, S. Kumar, T.S.N.S. Narayanan, J. Coat. Technol. Res. 9 (2012) 495–502, doi:10.1007/s11998-011-9382-6.
[127] M.R. Akbarpour, F. Farajnezhad, A.H. Poureshagh, S.Moniri Javadhesari, Inorg. Chem. 63 (2024) 20314–20324, doi:10.1021/acs.inorgchem.4c01841.
[128] E.C. Meng, S.K. Guan, H.X. Wang, L.G. Wang, S.J. Zhu, J.H. Hu, C.X. Ren, J.H. Gao, Y.S. Feng, Appl. Surf. Sci. 257 (2011) 4811–4816, doi:10.1016/j.apsusc.2010.12.073.
[129] H. Wang, S. Zhu, L. Wang, Y. Feng, X. Ma, S. Guan, Appl. Surf. Sci. 307 (2014) 92–100, doi:10.1016/j.apsusc.2014.03.172.
[130] H. Wang, S. Guan, Y. Wang, H. Liu, H. Wang, L. Wang, C. Ren, S. Zhu, K. Chen, Colloids. Surf. B Biointerfaces 88 (2011) 254–259, doi:10.1016/j.colsurfb.2011.06.040.
[131] L. Chen, Z. Zheng, J. Han, Z. Xu, C. Zhu, Russ. J. Phys. Chem. A 97 (2023) 1806–1815, doi:10.1134/S0036024423080149.
[132] W. Akram, R. Khan, M. Petrů, M. Amjad, K. Ahmad, M. Yasir, S. Ahmad, S.S. Rahimian Koloor, J. Mater. Res. Technol. 26 (2023) 2587–2600, doi:10.1016/J.JMRT.2023.08.026.
[133] R. Pani, R. Ranjan Behera, S. Roy, Electrophoretic deposition of hydroxyapatite coating: a state of art, Mater. Today Proc. 62 (2022) 4086–4093, doi:10.1016/j.matpr.2022.04.632.
[134] M.V. Smoluchowski, Zeitschrift Für Physikalische Chemie 92 (1903) 129–168.
[135] H.C. Hamaker, Physica 4 (1937) 1058–1072, doi:10.1016/S0031-8914(37)80203-7.
[136] R.M. Kumar, K.K. Kuntal, S. Singh, P. Gupta, B. Bhushan, P. Gopinath, D. Lahiri, Surf. Coat. Technol. 287 (2016) 82–92, doi:10.1016/j.surfcoat.2015.12.086.
[137] M. Aver, H. Pihtili, B. Aksakal, Ceram. Int. 51 (21) (2025) 35104–35118, doi:10.1016/j.ceramint.2025.05.235.
[138] Q. Tayyaba, M. Shahzad, A.Q. Butt, M.K. Rafi-ud-din, A.H. Qureshi, Surf. Coat. Technol. 375 (2019) 197–204, doi:10.1016/j.surfcoat.2019.07.014.
[139] R. Rojaee, M. Fathi, K. Raeissi, A. Sharifnabi, Ceram. Int. 40 (2014) 15149–15158, doi:10.1016/j.ceramint.2014.06.129.
[140] S. Singh, G. Singh, N. Bala, Mater. Today Commun. 26 (2021) 101870, doi:10.1016/j.mtcomm.2020.101870.
[141] A. Saadati, B.N. Khiarak, A.A. Zahraei, A. Nourbakhsh, H. Mohammadzadeh, Surf. Interfaces 25 (2021) 101290, doi:10.1016/j.surfin.2021.101290.
[142] Y. Gao, A. Yerokhin, A. Matthews, Surf. Coat. Technol. 269 (2015) 170–182, doi:10.1016/j.surfcoat.2015.01.030.
[143] S.A. Adeleke, S. Ramesh, A.R. Bushroa, Y.C. Ching, I. Sopyan, M.A. Maleque, S. Krishnasamy, H. Chandran, H. Misran, U. Sutharsini, Ceram. Int. 44 (2018) 1802–1811, doi:10.1016/j.ceramint.2017.10.114.
[144] F. Simchen, M. Sieber, A. Kopp, T. Lampke, Coatings 10 (7) (2020) 628, doi:10.3390/coatings10070628.
[145] C. Wen, X. Zhan, X. Huang, F. Xu, L. Luo, C. Xia, Surf. Coat. Technol. 317 (2017) 125–133, doi:10.1016/j.surfcoat.2017.03.034.
[146] H. Tang, W. Tao, C. Wang, H. Yu, RSC Adv. 8 (2018) 12368–12375, doi:10.1039/c7ra10951b.
[147] S. Mahmud, M. Rahman, M. Kamruzzaman, H. Khatun, M.O. Ali, M.M. Haque, Res. Eng. 17 (2023) 101002, doi:10.1016/j.rineng.2023.101002.
[148] A.S. Gnedenkov, S.L. Sinebryukhov, V.S. Filonina, S.V. Gnedenkov, J. Magnes. Alloys 11 (2023) 4468–4484, doi:10.1016/j.jma.2022.12.002.
[149] N. Usmaniya, S. R, P. V, R.K. L, R. N, J. Alloys Compd. 1004 (2024) 175723, doi:10.1016/j.jallcom.2024.175723.
[150] A. Keyvani, N. Kamkar, R. Chaharmahali, M. Bahamirian, M. Kaseem, A. Fattah-alhosseini, Inorg. Chem. Commun. 158 (2023) 111470, doi:10.1016/j.inoche.2023.111470.
[151] R. Chaharmahali, A. Fattah-Alhosseini, H. Esfahani, J. Asian Ceram. Soc. 8 (2020) 39–49, doi:10.1080/21870764.2019.1698143.
[152] C. Liu, W. Zhang, T. Xu, H. Li, B. Jiang, X. Miao, Ceram. Int. 48 (2022) 13676–13683, doi:10.1016/j.ceramint.2022.01.249.
[153] F. Momeni, M.R. Rahimipour, S.M.M. Khoeia, A. Zamanian, A. Massoudi, A. Ghanbari, Surf. Coat. Technol. 468 (2023) 129774, doi:10.1016/j.surfcoat.2023.129774.
[154] R.A. Surmenev, Surf. Coat. Technol. 206 (2012) 2035–2056, doi:10.1016/j.surfcoat.2011.11.002.
[155] V.S. Yadav, A. Kumar, A. Das, D. Pamu, L.M. Pandey, M.R. Sankar, Mater. Lett. 270 (2020) 127732, doi:10.1016/j.matlet.2020.127732.
[156] K. Lee, G. Shin, Arch. Metall. Mater. 60 (2015) 1319–1322, doi:10.1515/amm-2015-0122.
[157] K. Hirata, T. Kubota, D. Koyama, S. Takayanagi, M. Matsukawa, AIP Adv. 7 (2017) 085219, doi:10.1063/1.5000490.
[158] J.Z. Shi, C.Z. Chen, H.J. Yu, S.J. Zhang, Bull. Mater. Sci. 31 (2008) 877–884, doi:10.1007/s12034-008-0140-z.
[159] M.A. Surmeneva, T.M. Mukhametkaliyev, H. Khakbaz, R.A. Surmenev, M. Bobby Kannan, Mater. Lett. 152 (2015) 280–282, doi:10.1016/j.matlet.2015.03.140.
[160] T.M. Mukhametkaliyev, M.A. Surmeneva, A. Vladescu, C.M. Cotrut, M. Braic, M. Dinu, M.D. Vranceanu, I. Pana, M. Mueller, R.A. Surmenev, Mater. Sci. Eng. C 75 (2017) 95–103, doi:10.1016/j.msec.2017.02.033.
[161] L. Dragomir (Nicolescu), A. Antoniac, V. Manescu (Paltanea), A. Robu, M. Dinu, I. Pana, C.M. Cotrut, E. Kamel, I. Antoniac, J.V. Rau, A. Vladescu (Dragomir), Ceram. Int. 49 (2023) 26274–26288, doi:10.1016/j.ceramint.2023.05.116.
[162] A.C. Parau, C.M. Cotrut, P. Guglielmi, A. Cusanno, G. Palumbo, M. Dinu, G. Serratore, G. Ambrogio, D.M. Vranceanu, A. Vladescu, Ceram. Int. 48 (2022) 10486–10497, doi:10.1016/j.ceramint.2021.12.258.
[163] I. Pana, A.C. Parau, C.M. Cotrut, M. Dinu, D.M. Vranceanu, A.E. Kiss, G. Serratore, D.A. Böhner, C. Vitelaru, G. Ambrogio, A.G. Beck-Sickinger, A. Vladescu (Dragomir), Ceram. Int. 49 (2023) 22340–22354, doi:10.1016/j.ceramint.2023.04.064.
[164] V. Vishwakarma, G.S. Kaliaraj, K.K. Amirtharaj Mosas, Coatings 13 (1) (2023) 69, doi:10.3390/coatings13010069.
[165] A. Dehghanghadikolaei, B. Fotovvati, Materials 12 (2019) 1795, doi:10.3390/ma12111795.
[166] K. Fox, P.A. Tran, N. Tran, ChemPhysChem 13 (2012) 2495–2506, doi:10.1002/cphc.201200080.
[167] S. Shen, S. Cai, X. Bao, P. Xu, Y. Li, S. Jiang, G. Xu, Chem. Eng. J. 339 (2018) 7–13, doi:10.1016/j.cej.2018.01.083.
[168] J. Sun, S. Cai, J. Sun, K. Shen, J. Liu, G. Xu, Ultrason. Sonochem. 58 (2019) 104677, doi:10.1016/j.ultsonch.2019.104677.
[169] Y. Wang, X. Li, M. Chen, Y. Zhao, C. You, Y. Li, G. Chen, ACS Biomater. Sci. Eng. 5 (2019) 2858–2876, doi:10.1021/acsbiomaterials.9b00564.
[170] T. Wang, G. Yang, W. Zhou, J. Hu, W. Jia, W. Lu, J. Alloys Compd. 799 (2019) 71–82, doi:10.1016/j.jallcom.2019.05.338.
[171] X. Gu, W. Lin, D. Li, H. Guo, P. Li, Y. Fan, RSC Adv. 9 (2019) 15013–15021, doi:10.1039/c9ra02210d.
[172] W. Zhou, Z. Hu, T. Wang, G. Yang, W. Xi, Y. Gan, W. Lu, J. Hu, Colloids Surf. B Biointerfaces 186 (2020) 110710, doi:10.1016/j.colsurfb.2019.110710.

[173] S. Hiromoto, E. Nozoe, K. Hanada, T. Yoshimura, K. Shima, N. Nakamura, A. Chiba, Biomed. Mater. Devices 3 (2024) 1183–1199, doi:10.1007/s44174-024-00217-w.
[174] D. Sreekanth, N. Rameshbabu, Mater. Lett. 68 (2012) 439–442, doi:10.1016/j.matlet.2011.11.025.
[175] Z. Chen, W. Wang, Q. Liang, W. Lin, Int. J. Electrochem. Sci. 16 (2021) 211116, doi:10.20964/2021.11.04.
[176] R. Askarnia, S.R. Fardi, M. Sobhani, H. Staji, Ceram. Int. 47 (2021) 27071–27081, doi:10.1016/j.ceramint.2021.06.120.
[177] Z. Chunyan, C. Lan, L. Jiajia, S. Dongwei, Z. Jun, L. Huinan, J. Magnes. Alloys 10 (2022) 2252–2265, doi:10.1016/j.jma.2021.07.014.
[178] M. Tian, S. Cai, L. Ling, Y. Zuo, Z. Wang, P. Liu, X. Bao, G. Xu, Prog. Org. Coat. 165 (2022) 106745, doi:10.1016/j.porgcoat.2022.106745.
[179] L. Ling, S. Cai, Y. Zuo, M. Tian, T. Meng, H. Tian, X. Bao, G. Xu, Colloids Surf. B Biointerfaces 219 (2022) 112810, doi:10.1016/j.colsurfb.2022.112810.
[180] M. Zhang, S. Cai, S. Shen, G. Xu, Y. Li, R. Ling, X. Wu, J. Alloys Compd. 658 (2016) 649–656, doi:10.1016/j.jallcom.2015.10.282.
[181] T. Meng, S. Cai, L. Ling, Y. Zuo, H. Tian, H. Zhang, H. Zhang, G. Xu, Ceram. Int. 49 (2023) 25706–25715, doi:10.1016/j.ceramint.2023.05.117.
[182] Md.M. Rahman, R. Balu, A. Abraham, N.K. Dutta, N.R. Choudhury, ACS Appl. Bio. Mater. 4 (2021) 5542–5555, doi:10.1021/acsabm.1c00366.
[183] C.Y. Zhai, A. Ma, W. Wang, T. Zhu, L. Huanyu, W. Lan, T. Yu, J. Lan, Z. Wang, ACS Biomater. Sci. Eng. 11 (2025) 2290–2305, doi:10.1021/acsbiomaterials.4c02405.
[184] F.E.-T. Heakal, Y.B. Sarhan, M.A. Maamoun, A.M. Bakry, Y.K. Abdel-Monem, I.M. Ghayad, ACS Omega 7 (2022) 1021–1034, doi:10.1021/acsomega.1c05625.
[185] X.-J. Ji, L. Gao, J.-C. Liu, J. Wang, Q. Cheng, J.-P. Li, S.-Q. Li, K.-Q. Zhi, R.-C. Zeng, Z.-L. Wang, Colloids Surf. B Biointerfaces 179 (2019) 429–436, doi:10.1016/j.colsurfb.2019.04.029.
[186] J. Gao, Y.-K. Du, D. Jiang, Y.-Z. Liu, M. Li, K. Wang, L.-P. Che, S.-Q. Li, L.-Y. Cui, Y.-M. Xi, R.-C. Zeng, Mater. Today Commun. 40 (2024) 109592, doi:10.1016/j.mtcomm.2024.109592.
[187] B. Li, Y. Han, M. Li, J. Mater. Chem. B 4 (2016) 683–693, doi:10.1039/C5TB02101D.
[188] F.Z. Akbarzadeh, M. Rajabi, R. Jamaati, A. Braem, Corros. Sci. 245 (2025) 112678, doi:10.1016/J.CORSCI.2025.112678.
[189] J. Sun, S. Cai, J. Sun, K. Shen, J. Liu, G. Xu, Ultrason. Sonochem. 58 (2019) 104677, doi:10.1016/J.ULTSONCH.2019.104677.
[190] C.F. Dunne, G.K. Levy, O. Hakimi, E. Aghion, B. Twomey, K.T. Stanton, Surf. Coat. Technol. 289 (2016) 37–44, doi:10.1016/J.SURFCOAT.2016.01.045.
[191] M. Ahangari, M.H. Johar, M. Saremi, Ceram. Int. 47 (2021) 3529–3539, doi:10.1016/J.CERAMINT.2020.09.197.
[192] J. Chen, Y. Yang, I.P. Etim, L. Tan, K. Yang, R.D.K. Misra, J. Wang, X. Su, Materials 14 (2021) 5550, doi:10.3390/ma14195550.
[193] J. Park, S.H. Um, Y. Seo, J. Lee, Y.C. Kim, M.R. Ok, S.W. Hwang, J.Y. Sun, H.S. Han, H. Jeon, Bioact. Mater. 25 (2023) 796–806, doi:10.1016/J.BIOACTMAT.2022.06.020.
[194] T. Wu, K. Zhang, Coatings 13 (2023) 1533, doi:10.3390/COATINGS13091533.
[195] J.E. Gray, B. Luan, J. Alloys Compd. 336 (2002) 88–113, doi:10.1016/S0925-8388(01)01899-0.
[196] M.S. Safavi, F.C. Walsh, M.A. Surmeneva, R.A. Surmenev, J. Khalil-Allafi, Coatings 11 (2021) 110, doi:10.3390/coatings11010110.
[197] G. Prashar, H. Vasudev, L. Thakur, A. Bansal, Surf. Rev. Lett. 30 (2023) 2241001, doi:10.1142/S0218625X22410013.
[198] K. Qi, Y. Yang, G. Hu, X. Lu, J. Li, Surf. Coat. Technol. 397 (2020) 125983, doi:10.1016/J.SURFCOAT.2020.125983.
[199] R.I.M. Asri, W.S.W. Harun, M.A. Hassan, S.A.C. Ghani, Z. Buyong, J. Mech. Behav. Biomed. Mater. 57 (2016) 95–108, doi:10.1016/j.jmbbm.2015.11.031.
[200] M. Rafiei, H.E. Mohammadloo, M. Khorasani, F. Kargaran, H.A. Khonakdar, Heliyon 11 (2025) e41813, doi:10.1016/J.HELIYON.2025.E41813.
[201] H. Li, Z. Qin, Y. Ouyang, B. Zheng, H. Wei, J. Ou, C. Shen, J. Alloys. Compd. 909 (2022) 164694, doi:10.1016/J.JALLCOM.2022.164694.
[202] S. Hiromoto, E. Nozoe, K. Hanada, T. Yoshimura, K. Shima, T. Kibe, N. Nakamura, K. Doi, Mater. Sci. Eng. C 122 (2021) 111942, doi:10.1016/j.msec.2021.111942.
[203] D. Zhao, F. Witte, F. Lu, J. Wang, J. Li, L. Qin, Biomaterials 112 (2017) 287–302, doi:10.1016/j.biomaterials.2016.10.017.
[204] S.M. George, C. Nayak, I. Singh, K. Balani, ACS Biomater. Sci. Eng. 8 (2022) 3162–3186, doi:10.1021/acsbiomaterials.2c00140.
[205] R. Subbiah, M.A. Ruehle, B.S. Klosterhoff, A.S.P. Lin, M.H. Hettiaratchi, N.J. Willett, L.E. Bertassoni, A.J. García, R.E. Guldberg, Acta Biomater. 127 (2021) 180–192, doi:10.1016/J.ACTBIO.2021.03.066.
[206] O. Gherasim, A.M. Grumezescu, V. Grumezescu, I. Negut, M.F. Dumitrescu, M.S. Stan, I.C. Nica, A.M. Holban, G. Socol, E. Andronescu, Antibiotics 10 (2021) 160, doi:10.3390/antibiotics10020160.
[207] Q. qing Yi, P. chen Liang, D. yu Liang, J. feng Shi, S. Sha, Q. Chang, Ceram. Int. 47 (2021) 8133–8141, doi:10.1016/J.CERAMINT.2020.11.168.
[208] N. Singh, U. Batra, K. Kumar, N. Ahuja, A. Mahapatro, Bioact. Mater. 19 (2023) 717–757, doi:10.1016/J.BIOACTMAT.2022.05.009.
[209] B. Beig, U. Liaqat, M.F.K. Niazi, I. Douna, M. Zahoor, M.B.K. Niazi, Coatings 10 (2020) 1249, doi:10.3390/coatings10121249.
[210] R. Pani, R. Ranjan Behera, S. Roy, Mater. Today. Proc. 62 (2022) 4086–4093, doi:10.1016/J.MATPR.2022.04.632.
[211] G. Wang, Y. Zhu, X. Zan, M. Li, Front. Bioeng. Biotechnol. 9 (2021) 718255, doi:10.3389/fbioe.2021.718255.
[212] H.R. Bakhsheshi-Rad, E. Hamzah, A.F. Ismail, M. Aziz, M. Daroonparvar, E. Saebnoori, A. Chami, Surf. Coat. Technol. 334 (2018) 450–460, doi:10.1016/j.surfcoat.2017.11.027.
[213] X. Fu, L. Tian, Y. Fan, W. Ye, Z.A. Qiao, J. Zhao, L. Ren, W. Ming, Mater. Today Chem. 22 (2021) 100575, doi:10.1016/J.MTCHEM.2021.100575.
[214] M.U. Joshi, S.P. Kulkarni, M. Choppadandi, M. Keerthana, G. Kapusetti, Smart Mater. Med. 4 (2023) 661–679, doi:10.1016/j.smaim.2023.06.005.
[215] X. Ni, Y. Gao, X. Zhang, Y. Lei, G. Sun, B. You, Chem. Eng. J. 406 (2021) 126725, doi:10.1016/J.CEJ.2020.126725.
[216] A. Nelson, Nat. Mater. 7 (2008) 523–525, doi:10.1038/NMAT2214.
[217] Y. Li, D. Lau, Giant 18 (2024) 100277, doi:10.1016/J.GIANT.2024.100277.
[218] G.L. Koons, M. Diba, A.G. Mikos, Nat. Rev. Mater. 5 (2020) 584–603, doi:10.1038/S41578-020-0204-2.
[219] W. Wang, L. Wang, B. Zhang, S. Shang, C. Zhao, W. Zhang, J. Chen, C. Zhou, H. Zhou, S. Feng, Chem. Eng. J. 484 (2024) 149444, doi:10.1016/J.CEJ.2024.149444.
[220] A. Kumar, S. Kargozar, F. Baino, S.S. Han, Front. Mater. 6 (2019) 333, doi:10.3389/fmats.2019.00313.
[221] H. Khatun, M. Rahman, S. Mahmud, M.O. Ali, M. Akter, Res. Eng. 18 (2023) 101162, doi:10.1016/J.RINENG.2023.101162.
[222] Z. Ran, Y. Wang, J. Li, W. Xu, J. Tan, B. Cao, D. Luo, Y. Ding, J. Wu, L. Wang, K. Xie, L. Deng, P. Fu, X. Sun, L. Shi, Y. Hao, Int. J. Bioprint. 9 (2023) 769, doi:10.18063/ijb.769.
[223] Z. Wang, Y. Sun, C. Li, Front. Bioeng. Biotechnol. 12 (2024) 1483547, doi:10.3389/fbioe.2024.1483547.